Covert Communications in STAR-RIS Assisted NOMA Networks over Nakagami-m Fading Channels

Qiang Li, *Student Member, IEEE*, Dongyang Xu, *Member, IEEE*, Keyue Zhang, Keivan Navaie, *Senior Member, IEEE* and Zhiguo Ding, *Fellow, IEEE*

***Abstract*—Combination of simultaneously transmitting and reflecting-reconfigurable intelligent surface (STAR-RIS) and Non-orthogonal multiple (NOMA) brings the necessary full-space degrees of freedom and spatial multiplexing gains for the internet of things (IoT) networks. Meanwhile, the introduced network heterogeneity and sharing of channels make the information interactions more exposed. To mitigate the flaw, this paper proposes a covert communication scheme in STAR-RIS assisted NOMA networks over Nakagami-m fading channels for downlink and uplink IoT scenarios. Under the NOMA protocol with imperfect successive interference cancellation (SIC), an IoT access point aims to achieve the information interactions with two IoT users aided by a STAR-RIS, without being detected by two wardens. The two IoT users are located on both sides of the STAR-RIS, which adopts the coherent phase shifting and works in the mode switching protocol. In the scheme, Kullback-Leibler (KL) divergence is used for evaluating the detection performance of wardens. The cascade channel gains of IoT users and wardens are respectively characterized as Gamma and complex Gaussian random variables. Upon this, the close-form expressions of the expectations of KL divergence and the interruption probabilities for downlink and uplink scenarios are derived. To improve the performance, by jointly optimizing the transmit power and power allocation coefficient, the effective covert rate maximization problems are formulated for downlink and uplink scenarios, subject to covertness, reliability and power boundary constraints, which are respectively resolved analytically. Numerical results are provided to demonstrate that the proposed scheme can bring more covertness gain compared with benchmarks.**

***Index Terms*—Internet of things (IoT), reconfigurable intelligence surface (RIS), simultaneously transmitting and reflecting (STAR), non-orthogonal multiple (NOMA), covert communications.**

I. Introduction

The past decade has witnessed the revolutionary progress of the communication technologies, which is already evolving to the sixth generation (6G) wireless communication networks. The first 6G white paper, entitled "Vision of 6G wireless systems: applications, trends, technologies, and open research problems", pointed out that 6G networks would achieve the high reliability, high bandwidth, high security, high transmission speed and low delay communications [1]. These features facilitate the emerging internet of things (IoT) application scenarios, such as remote surgery, smart homes, intelligent transportation and smart cities, which will resultantly proliferate the exponential IoT terminals and ubiquitous personalized services [2]. It is predicted that there will be 75 billion IoT devices connected to the IoT networks by 2030, which brings tremendous challenges for the existing networks in terms of network performance, resources and architecture [3], [4]. How to support the multiple access, high security, sufficient coverage, and lower resource consumption communication in the IoT networks has attracted a lot of attention from researchers.

Non-orthogonal multiple access (NOMA) and reconfigurable intelligent surface (RIS) have been deemed as two potential technologies to cope with the mentioned challenges [5]. In one respect, NOMA can accommodate multiple services in parallel by splitting them into different power domains to perform the successive interference cancellation (SIC), which adequately improves spectral efficiency, is in favor of massive connectivity and lets transmission delay down [6]. Due to these capabilities, NOMA has been widely applied in the IoT scenarios, such as massive machine type communications (mMTC), unmanned aerial vehicle (UAV) communications and ultra-reliable low-latency communications (uRLLC) [7]–[9]. In other respects, RIS consists of a large number of passive particle metamaterial elements, each of which can independently reconfigure the properties of the incident signals, i.e., phase and amplitude, controlled by a smart controller [10]. With extremely low cost and power consumption, RIS can improve the spatial diversity gain, expand the transmission coverage and create favorable propagation environments for received electromagnetic waves [11]. With these strengths, RIS is arranged in the IoT networks to improve channel capacities, save transmission costs and relay long-distance transmissions et cetera [12]–[14].

A. Literatures Review

Benefitting from these capabilities, applying the potentials of RIS into NOMA IOT networks has recently become a hot research topic. [15] and [16] characterized the reliability improvement for RIS-assisted NOMA networks. Considering

Manuscript received XXX, XX, 2023; revised XXX, XX, 2023.

Q. Li and D. Xu are with the School of Information and Communications Engineering, Xi'an Jiaotong University, Xi'an 710049, China. (e-mail: liqiang16@stu.xjtu.eud.cn, xudongyang@xjtu.edu.cn)

K. Zhang is with the School of Microelectronics, Xi'an Jiaotong University, Xi'an 710049, China. (e-mail: penny007@stu.xjtu.edu.cn)

K. Navaie is with the School of Computing and Communications, Lancaster University, LA1 4WA Lancaster, U.K. (e-mail: k.navaie@lancaster.ac.uk)

Z. Ding is with the Department of Electrical Engineering and Computer Science, Khalifa University, Abu Dhabi, UAE. (e-mail: zhiguo.ding@manchester.ac.uk)

the power consumption and sum rate tradeoff, Wang et al. proposed a energy efficiency maximization strategy for RIS NOMA networks in [17]. By optimizing the phase of RIS, the authors of [18] proposed a machine learning based throughput maximization scheme for RIS aided NOMA IoT networks. It is worth mentioning that RIS requires all served users to be located on the same side of RIS, which degrades the degrees of freedom. To overcome this bottleneck, simultaneously transmitting and reflecting (STAR)-RIS was introduced. Each element of STAR-RIS can reflect and refract the incident signals in parallel under the protocols of power splitting, mode switching or time switching, which provides the full-space (i.e., 360°) coverage for IoT networks [19]. It was validated in [20] that STAR-RIS could significantly extend the coverage compared with RIS. Upon this, Du et al. established a wireless powered IoT transmission transmission framework by means of STAR-RIS in [21].

Further, the combination of STAR-RIS and NOMA IoT networks has aroused the interest of researchers. [22] provided a general analytical framework for the STAR-RIS based NOMA network, in which coverage probability and average transmission rates of users were characterized. Wang et al. pointed out that the received signal to noise ratios (SNR) of NOMA users were maximized when the coherent phase shifting was adopted at STAR-RIS [23]. By optimizing the decoding order of IoT terminals and phases of STAR-RIS, the authors of [24] maximized the effective sum rate of NOMA IoT networks. As compared with orthogonal multiple access (OMA), [25] validated applying STAR-RIS into multiple-input and multiple-output (MIMO) NOMA networks could yield higher energy efficiency gains. By adjusting the deployment location of STAR-RIS, the weighted throughput of NOMA networks was optimized [26]. [27] deployed the STAR-RIS NOMA in UAV networks, which maximized the sum rate of networks by optimizing the location of UAV and phases of STAR-RIS.

Owing to the openness and sharing of IoT transmission medium, the transmitted information is directly exposed in the networks. For security-sensitive contents, they tend not to be effectively monitored by other nodes. For instance, in unmanned remote control system, in case they are detected and then jammed, control commands are expected to be conveyed covertly. Covert communication, aiming at achieving the information transmissions without being detected by malicious wardens, was introduced to remedy the vacancy. With the help of relay, the authors of [28] achieved covert transmissions in IoT networks. [29]–[32] investigated covert communication in NOMA networks. These literatures confused the wardens by creating uncertainty to wardens by means of channel inversion power control [29], random transmit power [30], uncertain channel distribution information [31] and extra imposed jamming [32]. Those eventually increased the detection error probabilities of wardens so that wardens could not effectively tell whether the communication occurred. In [33], the authors utilized the Kullback-Leibler (KL) divergence to characterize the detection performance of wardens, which provided a novel paradigm for covert communication design.

More recently, the covert communication in RIS IoT networks has also been extensively explored. In [34], Ma et al. considered the covert transmission in RIS-assisted IoT networks, in which two covert rate maximization strategies were proposed with and without the channel state information (CSI) of warden. The authors of [35] investigated an energy-efficient covert UAV communication scheme over terahertz (THz) band with the help of RIS, which improved the covert throughput. Considering the information freshness, [36] proposed an opportune two-way information exchange protocol for RIS aided networks. Considering residual hardware impairments, Chen et al. in [37] maximized the network capacity under the constraint of the covertness by jointly optimizing the transmit power and phase of RIS for RIS IoT networks. By introducing phase uncertainty from RIS, [38] achieved the covert uplink and downlink transmission for RIS aided NOMA networks. In [39], the authors jointly considered the security and covertness for RIS assisted NOMA networks, in which secrecy outage probability and detection error probability were characterized.

B. Motivations and Contributions

As for the aforementioned research efforts, we summarize the significant observations below.

1. In the existing literatures on covert communication in NOMA networks [29]–[32], [38], [39], it is assumed that there are two users in NOMA networks. One of them is a public user and the other is a covert user. Regardless of covert action, public user always sends information to provide a shelter, which is resources-wasting without necessary public action. Therefore, it is necessary to investigate the covert communication of the NOMA network as a whole.
2. For the IoT node far away from the IoT access point [28], the relay is deployed to assist covert transmission. The relay divides the covert action into two phases, which provides warden another opportunity for detection. Simultaneously, the increased power by the relay makes information transmission more exposed, which is unfriendly to remote covert action.
3. In the existing works on covert RIS transmission [34]–[39], it is required that all users are located at the same side of RIS, which decreases the degrees of freedom and only provides half-space covert transmission. For users on the opposite side of RIS, covert communication is unlikely to be achieved.

Inspired by these observations, this paper considers the covert communication in STAR-RIS assisted NOMA networks for downlink and uplink IoT scenarios, for the first time. Under the NOMA protocol with the imperfect SIC, an IoT access point aims at covertly completing the information interactions with two IoT users, each of which is monitored by a warden, aided by a STAR-RIS. The two IoT users are located on both sides of the STAR-RIS. Similar to [23], the coherent phase shifting is adopted at STAR-RIS working in the mode switching protocol, which can maximize the received SNRs of IoT users. Our goal is to hide the entire interactions of

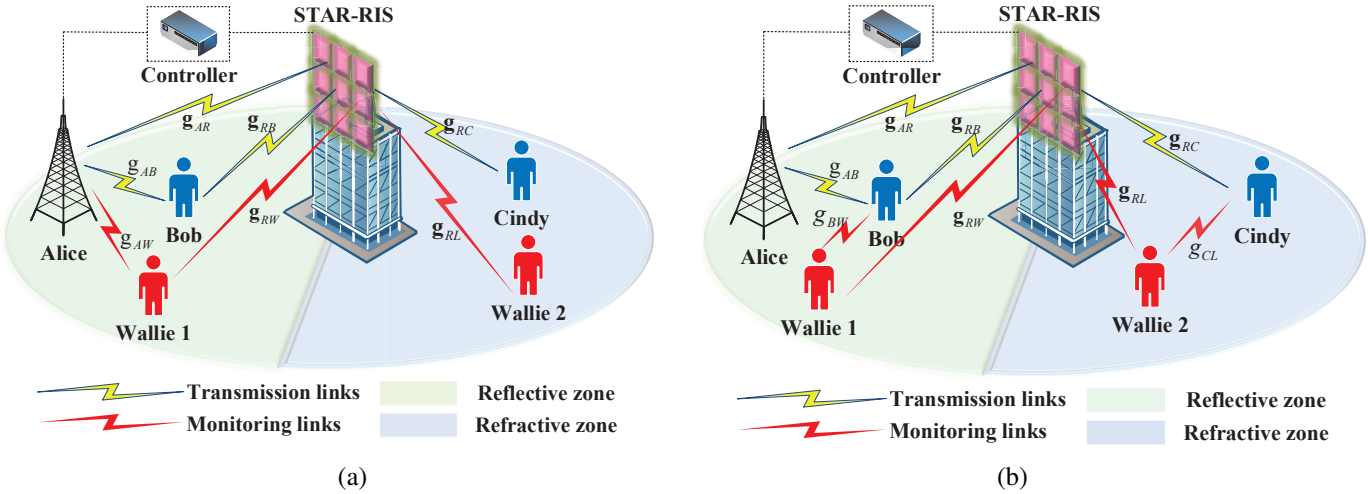

Fig. 1. System model for STAR-RIS assisted NOMA Networks. (a) Downlink IoT scenario. (b) Uplink IoT scenario.

STAR-RIS assisted NOMA networks. More particularly, our main contributions are fourfold:

1. We propose a novel covert STAR-RIS assisted NOMA transmission scheme over Nakagami-m fading channels for downlink and uplink IoT scenarios. Considering the worst case, wardens can have access to all CSI of the network but only statistical CSI of wardens is available at the IoT access point. In the scheme, the phase shifting of STAR-RIS provides a shelter for the covert actions and KL divergence is utilized to analyze the detection performance of wardens.
2. For the proposed scheme, we provide an analytical framework for covertness and reliability of the networks. The cascade channels gains of the IoT users are characterized as two random variables (RV) following Gamma distribution. The cascade channels gains of wardens are approximated as two complex Gaussian RV. As a result, the close-form expressions of the expectations of KL divergence and transmission interruption probabilities under the imperfect SIC for downlink and uplink IoT scenarios are derived.
3. In order to improve the performance, we formulate the effective covert rate (ECR) maximization problems, subject to covertness demands, reliability constraints and power boundary constraints. For the downlink IoT scenario, by jointly optimizing the transmit power and power allocation coefficient of the IoT access point, the maximum ECR is captured analytically. For the uplink IoT scenario, by joint optimizing the transmit power of two IoT users, the maximum ECR is acquired by a 2D numerical search.
4. Numerical results are preened to demonstrate that applying the potentials of STAR-RIS into NOMA networks can bring more covertness gain, as compared with benchmarks.

The rest of the paper is organized as follows: Sect. II introduces the system and channels models for the STAR-RIS assisted NOMA networks for downlink and uplink IoT scenarios. Sect. III analyzes jointly the information transmissions, covertness, and covert scheme design for the downlink scenarios. Sect. IV details jointly the information transmissions, covertness and covert scheme design for the uplink scenarios. Numerical results are provided to demonstrate the superiority of the proposed principle as compared with the benchmarks in Sect. V. Finally, Sect. VI concludes the paper.

TABLE I
ACRONYMS AND MEANINGS

Abbreviations	Descriptions
AWGN	additive white Gaussian noise
CSI	channel state information
IoT	internert of things
KL	Kullback-Leibler
MDEP	minimum detection error probability
NOMA	non-orthogonal multiple access
RIS	reconfigurable intelligent surface
RV	random variable
SIC	successive interference cancellation
SNR(SINR)	signal to (interference and) noise ratio
STAR	simultaneously transmitting and reflecting

Notations: The uppercase and lowercase boldface letters serve as the matrixes and vectors, respectively. $X \sim f(x)$ shows that probability density function (pdf) of X is $f(x)$. $\mathcal{CN}(a,b)$ and $\mathcal{N}(a,b)$ respectively denote the circular symmetric complex Gaussian distribution and Gaussian distribution with mean a and variance b. $\Gamma(k,\theta)$ and $U(a,b)$ respectively mean Gamma distribution with shape parameter k and scale parameter θ and uniform distribution over the interval (a,b). $\text{diag}(\cdot) \in \mathbb{C}^{K\times K}$ means $K \times K$ diagonal matrix. $\mathbb{E}(\cdot)$, $\mathbb{V}(\cdot)$ and $\mathbb{P}(\cdot)$ respectively denote the expectation, variance and probability operations. Some main abbreviations used below and their descriptions are summarized in the Table I.

II. System and Channel Models

This paper considers the covert transmissions in the STAR-RIS assisted NOMA networks for downlink and uplink IoT scenarios, as exhibited in Fig. 1. Using the NOMA protocol, an

IoT access point, termed as Alice, aims to covertly complete information interaction with two IoT users, termed as Bob and Cindy, which are monitored by two wardens, termed as Willie 1 and Willie 2. The wardens are likely to be idle IoT nodes. From the distance to Alice, Bob and Cindy are the near and far terminals, respectively. Due to tall obstacles, there is no direct communication link between Alice and Cindy. To facilitate the transmissions, a STAR-RIS capable of both reflecting and refracting the incident signals is deployed in the networks. The STAR-RIS consists of $2K$ reconfigurable elements, each of which can reflect or refract the signals on its own. The STAR-RIS is controlled by Alice through a smart controller adjusting the parameters of all elements. For the convenience of deployment, it is assumed that the STAR-RIS works in the mode switching protocol and divides its $2K$ elements into two equal parts for the reflection and refraction, in which the corresponding regions are called the reflective and refractive zones. As such, Bob and Willie 1 are located at the reflective zone while Cindy and Willie 2 are located at the refractive zone. As long as one of Willie 1 and Willie 2 can detect communication behaviours, the covert transmissions are suspended. All terminals with single antenna work in the half-duplex mode.

Assume that the channels associated with the STAR-RIS undergo independently distributed (i.d.) Nakagami-m fading along with path loss. The channels of direct links are captured by the Rayleigh fading along with path loss. Let d_{AB}, d_{AW}, d_{BW}, d_{CL}, d_{AR}, d_{RB}, d_{RW}, d_{RC} and d_{RL} denote the distances of links Alice $\rightarrow$ Bob, Alice $\rightarrow$ Willie 1, Bob $\rightarrow$ Willie 1, Cindy $\rightarrow$ Willie 2, Alice $\rightarrow$ STAR-RIS, STAR-RIS $\rightarrow$ Bob, STAR-RIS $\rightarrow$ Willie 1, STAR-RIS $\rightarrow$ Cindy and STAR-RIS $\rightarrow$ Willie 2, respectively. The corresponding small-scale fading coefficients are respectively expressed as g_{AB}, g_{AW}, g_{BW}, g_{CL}, $\mathbf{g}_{AR}$, $\mathbf{g}_{RB}$, $\mathbf{g}_{RW}$, $\mathbf{g}_{RC}$ and $\mathbf{g}_{RL}$, where $g_{AB}, g_{AW}, g_{BW}, g_{CL} \sim \mathcal{CN}(0,1)$, $\mathbf{g}_{\Delta} \in \mathbb{C}^{K\times 1}$ and $|g_{\Delta,k}| \sim Nakagami(m_{\Delta}, 1)$, $\Delta \in \{AR, RB, RW, RC, RL\}$, $k \in [1, K]$ and $|g_{\Delta,k}|$ means of the modulus of k-th entry of $\mathbf{g}_{\Delta}$. The large-scale path loss coefficients are captured by $L_{\Upsilon} = L_0 d_{\Upsilon}^{-\beta}$, where $\Upsilon \in \{\Delta, AB, AW, BW, CL\}$, β is the path loss exponent and L_0 means the reference path loss per unit distance. Regarding channel information, we have the following assumptions: 1) Channel condition of Bob is better than that of Cindy, based on that Bob and Cindy are near and far users in terms of distance to Alice. 2) Alice knows the instantaneous CSI of links Alice-Bob and Alice-RIS-users based on channel estimation. Only statistical CSI of links related to wardens are available at Alice, because wardens cannot feed back their instantaneous CSI. 3) Channel reciprocity is hold in the networks. To support this, the networks work in the time-division duplexing (TDD) mode for the downlink and uplink communications. 4) Wardens can have access to CSI of all links, which is the worst case.

III. Covert Communications in STAR-RIS Downlink NOMA Networks

In this section, we consider the covert communications in STAR-RIS assisted downlink NOMA networks. First, we analyze the information transmission of the downlink NOMA networks. Then, we detail the covertness of the networks. Last, the covert transmission scheme is designed.

A. STAR-RIS Assisted Downlink NOMA Transmissions

As shown in Fig. 1(a), in the downlink NOMA networks, Alice transmits two unit-power covert signals x_B and x_C to Bob and Cindy with the help of a STAR-RIS. The received signals at Bob and Cindy can be denoted by

$$y_B[m] = \left(\sqrt{L_{AB}}g_{AB} + \sqrt{L_{AR}L_{RB}}\mathbf{g}_{RB}^H \mathbf{\Theta}_R \mathbf{g}_{AR}\right) \times \left(\sqrt{a_1 P_A}x_B[m] + \sqrt{a_2 P_A}x_C[m]\right) + n_B[m], \tag{1}$$

and

$$y_C[m] = \sqrt{L_{AR}L_{RB}}\mathbf{g}_{RC}^H \mathbf{\Theta}_T \mathbf{g}_{AR} \times \left(\sqrt{a_1 P_A}x_B[m] + \sqrt{a_2 P_A}x_C[m]\right) + n_C[m], \tag{2}$$

where P_A is the transmit power at Alice. a_1 and a_2 with $a_1 + a_2 = 1$ are the power allocation factors of Alice. Bob has better channel condition, so $0 < a_1 < 0.5$ is assumed. $n_B \sim \mathcal{CN}(0, \sigma_B^2)$ and $n_C \sim \mathcal{CN}(0, \sigma_C^2)$ are the additive white Gaussian noises (AWGN) at Bob and Cindy, respectively. m is the index of channel use for the occupied slot. $\mathbf{\Theta}_R = \text{diag}\left(e^{j\theta_1^R}, ..., e^{j\theta_k^R}, ..., e^{j\theta_K^R}\right) \in \mathbb{C}^{K\times K}$ and $\mathbf{\Theta}_T = \text{diag}\left(e^{j\theta_1^T}, ..., e^{j\theta_k^T}, ..., e^{j\theta_K^T}\right) \in \mathbb{C}^{K\times K}$ denote the reflection and refraction coefficients matrixes with $\theta_k^R, \theta_k^T \in [0, 2\pi)$ being the phase shift of k-th element of the STAR-RIS regulated by Alice. In the NOMA network, Bob first decode x_C and then extract x_B by removing the partial x_C. Consider the imperfect SIC, the signal to interference and noise ratio (SINR) extracting x_C and SNR decoding x_B at Bob can be given by

$$\gamma_{B,C} = \frac{|\sqrt{L_{AB}}g_{AB} + \sqrt{L_{AR}L_{RB}}\mathbf{g}_{RB}^H \mathbf{\Theta}_R \mathbf{g}_{AR}|^2 a_2 P_A}{|\sqrt{L_{AB}}g_{AB} + \sqrt{L_{AR}L_{RB}}\mathbf{g}_{RB}^H \mathbf{\Theta}_R \mathbf{g}_{AR}|^2 a_1 P_A + \sigma_B^2}, \tag{3}$$

and

$$\gamma_B = \frac{|\sqrt{L_{AB}}g_{AB} + \sqrt{L_{AR}L_{RB}}\mathbf{g}_{RB}^H \mathbf{\Theta}_R \mathbf{g}_{AR}|^2 a_1 P_A}{\phi|\sqrt{L_{AB}}g_{AB} + \sqrt{L_{AR}L_{RB}}\mathbf{g}_{RB}^H \mathbf{\Theta}_R \mathbf{g}_{AR}|^2 a_2 P_A + \sigma_B^2}, \tag{4}$$

respectively. Where $0 \leq \phi < 1$ is the iSIC factor with $\phi = 0$ meaning the perfect SIC. Regarding x_B as the interference, the SNR of Cindy directly decoding x_C can be given by

$$\gamma_C = \frac{|\sqrt{L_{AR}L_{RC}}\mathbf{g}_{RC}^H \mathbf{\Theta}_T \mathbf{g}_{AR}|^2 a_2 P_A}{|\sqrt{L_{AR}L_{RC}}\mathbf{g}_{RC}^H \mathbf{\Theta}_T \mathbf{g}_{AR}|^2 a_1 P_A + \sigma_C^2}. \tag{5}$$

Having no access to instantaneous CSI of wardens, Alice regulates $\mathbf{\Theta}_R$ and $\mathbf{\Theta}_T$ in line with the channel information of users. As pointed out in [22], a coherent phase shift strategy can maximize the SNRs of both users. In this case, the optimal θ_k^R can θ_k^T can be given by

$$\left(\theta_k^R\right)^* = \theta_{AB} - (\theta_{RB,k} + \theta_{AR,k}), \tag{6}$$

and

$$\left(\theta_k^T\right)^* = -(\theta_{RC,k} + \theta_{AR,k}), \tag{7}$$

respectively. θ_{AB} and $\theta_{\Delta,k}$ denote the phases of g_{AB} and k-th entry of $\mathbf{g}_\Delta$, respectively. The optimal reflection and refraction coefficients matrixes can be respectively given by

$$\mathbf{\Theta}_R^* = \text{diag}\left(e^{j\left(\theta_1^R\right)^*}, ..., e^{j\left(\theta_k^R\right)^*}, ..., e^{j\left(\theta_K^R\right)^*}\right), \tag{8}$$

and

$$\mathbf{\Theta}_T^* = \text{diag}\left(e^{j\left(\theta_1^T\right)^*}, ..., e^{j\left(\theta_k^T\right)^*}, ..., e^{j\left(\theta_K^T\right)^*}\right). \tag{9}$$

B. Covertness Analysis of STAR-RIS Downlink NOMA

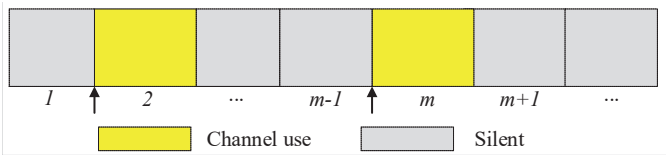

Fig. 2. Channel use diagram of selected transmission slot.

1) Detection at Wardens: To avoid being detected by wardens, Alice cannot always transmit the signals in each slot. As shown in Fig. 2, Alice sends the covert information with a certain prior probability ρ in a selected slot. As such, wardens are not sure whether the covert signals are sent. They need to make a binary judgement in line with their observations in the network. Let $\mathcal{H}0$ and $\mathcal{H}1$ denote respectively that Alice sends and does not send the covert signals to NOMA users. Under $\mathcal{H}0$ and $\mathcal{H}1$, the received signals at Willie 1 and Willie 2 can be given as follows:

$$\begin{cases} \mathcal{H}0: y_{W1}[m] = n_{W1}[m], \\ \mathcal{H}0: y_{W2}[m] = n_{W2}[m], \\ \mathcal{H}1: y_{W1}[m] = \left(\sqrt{L_{AW}}g_{AW} + \sqrt{L_{AR}L_{RW}}\mathbf{g}_{RW}^H\mathbf{\Theta}_R\mathbf{g}_{AR}\right) \\ \quad \times \left(\sqrt{a_1P_A}x_B[m] + \sqrt{a_2P_A}x_C[m]\right) + n_{W1}[m], \\ \mathcal{H}1: y_{W2}[m] = \sqrt{L_{AR}L_{RL}}\mathbf{g}_{RL}^H\mathbf{\Theta}_T\mathbf{g}_{AR} \\ \quad \times \left(\sqrt{a_1P_A}x_B[m] + \sqrt{a_2P_A}x_C[m]\right) + n_{W2}[m]. \end{cases} \tag{10}$$

Wherein, $n_{W1} \sim \mathcal{CN}(0, \sigma_{W1}^2)$ and $n_{W2} \sim \mathcal{CN}(0, \sigma_{W2}^2)$ denote the AWGN at Willie 1 and Willie 2, respectively. m is the index of channel use for the occupied slot. Without loss of generality, $\sigma_B^2 = \sigma_C^2 = \sigma_0^2$ and $\sigma_{W1}^2 = \sigma_{W2}^2 = \sigma_W^2$ are set. Assume that Alice chooses to send covert signals or not with equal prior probability, i.e., $\rho = 0.5$. To maximize the detection performance, wardens adopt the optimal test strategy. The corresponding minimum detection error probability (MDEP) can be computed by [33]

$$\Xi^* = 1 - \mathcal{V}_T\left(\mathbb{P}_0^{W1/W2}, \mathbb{P}_1^{W1/W2}\right), \tag{11}$$

where $\mathcal{V}_T\left(\mathbb{P}_0^{W1/W2}, \mathbb{P}_1^{W1/W2}\right)$ is the total variation distance between $\mathbb{P}_0^{W1/W2}$ and $\mathbb{P}_1^{W1/W2}$ being the probability distributions of received signals at Willie 1/Willie 2 under $\mathcal{H}0$ and $\mathcal{H}1$ shown as follows: $\mathbb{P}_0^{W1} \triangleq f(y_{W1}[m]|\mathcal{H}0) = \mathcal{CN}(0, \sigma_W^2)$, $\mathbb{P}_0^{W2} \triangleq f(y_{W2}[m]|\mathcal{H}0) = \mathcal{CN}(0, \sigma_W^2)$, $\mathbb{P}_1^{W1} \triangleq f(y_{W1}[m]|\mathcal{H}1) = \mathcal{CN}(0, P_A|\sqrt{L_{AW}}g_{AW} + \sqrt{L_{AR}L_{RW}}\mathbf{g}_{RW}^H\mathbf{\Theta}_R\mathbf{g}_{AR}|^2 + \sigma_W^2)$ and $\mathbb{P}_1^{W2} \triangleq f(y_{W2}[m]|\mathcal{H}1) = \mathcal{CN}(0, P_A|\sqrt{L_{AR}L_{RL}}\mathbf{g}_{RL}^H\mathbf{\Theta}_T\mathbf{g}_{AR}|^2 + \sigma_W^2)$. Since $\mathcal{V}_T\left(\mathbb{P}_0^{W1/W2}, \mathbb{P}_1^{W1/W2}\right)$ is difficult to handle, by the Pinskers inequality [33], an analyzable upper bound is acquired by

$$\mathcal{V}_T\left(\mathbb{P}_0^{W1/W2}, \mathbb{P}_1^{W1/W2}\right) \leq \sqrt{0.5\mathcal{D}\left(\mathbb{P}_0^{W1/W2} \parallel \mathbb{P}_1^{W1/W2}\right)}, \tag{12}$$

where $\mathcal{D}\left(\mathbb{P}_0^{W1/W2} \parallel \mathbb{P}_1^{W1/W2}\right)$ is the KL divergence from $\mathbb{P}_0^{W1/W2}$ to $\mathbb{P}_1^{W1/W2}$, which can be respectively calculated by

$$\begin{aligned} \mathcal{D}_{W1} &= \mathcal{D}\left(\mathbb{P}_0^{W1} \parallel \mathbb{P}_1^{W1}\right) \\ &= \int_x f(y_{W1}(x)[m]|\mathcal{H}0) \ln \frac{f(y_{W1}(x)[m]|\mathcal{H}0)}{f(y_{W1}(x)[m]|\mathcal{H}1)} dx \\ &\overset{(a)}{=} \ln\left(1 + \frac{\sigma_{\nu_1}^2}{\sigma_W^2}\right) + \frac{\sigma_W^2}{\sigma_{\nu_1}^2 + \sigma_W^2} - 1, \end{aligned} \tag{13}$$

and

$$\begin{aligned} \mathcal{D}_{W2} &= \mathcal{D}\left(\mathbb{P}_0^{W2} \parallel \mathbb{P}_1^{W2}\right) \\ &= \int_x f(y_{W2}(x)[m]|\mathcal{H}0) \ln \frac{f(y_{W2}(x)[m]|\mathcal{H}0)}{f(y_{W2}(x)[m]|\mathcal{H}1)} dx \\ &\overset{(a)}{=} \ln\left(1 + \frac{\sigma_{\nu_2}^2}{\sigma_W^2}\right) + \frac{\sigma_W^2}{\sigma_{\nu_2}^2 + \sigma_W^2} - 1, \end{aligned} \tag{14}$$

where (a) means substituting the expressions of the probability distributions into the integral. $\sigma_{\nu_1}^2$ and $\sigma_{\nu_1}^2$ can be respectively given by

$$\sigma_{\nu_1}^2 = P_A \mid \sqrt{L_{AW}}g_{AW} + \sqrt{L_{AR}L_{RW}}\mathbf{g}_{RW}^H\mathbf{\Theta}_R\mathbf{g}_{AR} \mid^2, \tag{15}$$

and

$$\sigma_{\nu_2}^2 = P_A \mid \sqrt{L_{AR}L_{RL}}\mathbf{g}_{RL}^H\mathbf{\Theta}_T\mathbf{g}_{AR} \mid^2. \tag{16}$$

Substituting (12) into (11), it is acquired that the MDEP satisfy

$$\Xi^* \geq 1 - \sqrt{0.5\mathcal{D}\left(\mathbb{P}_0^{W1/W2} \parallel \mathbb{P}_1^{W1/W2}\right)}. \tag{17}$$

Generally, covert communication is achieved when $\Xi^* \geq 1 - \varepsilon$ for a given arbitrarily small value of $\varepsilon > 0$ being depending on covertness level. Substituting it into (17), we can reacquire the covertness constraint as

$$\mathcal{D}\left(\mathbb{P}_0^{W1/W2} \parallel \mathbb{P}_1^{W1/W2}\right) \leq 2\varepsilon^2. \tag{18}$$

2) Expected Detection Performance: Having no access to the instantaneous CSI related to wardens, Alice has no idea about specific values of $\sigma_{\nu_2}^1$ and $\sigma_{\nu_2}^2$. We utilize the expected values of $\mathcal{D}\left(\mathbb{P}_0^{W1/W2} \parallel \mathbb{P}_1^{W1/W2}\right)$ over all channel realizations of wardens to evaluate covertness of the networks in this paper.

Lemma 1: When K is sufficiently large, $\xi_W = \mathbf{g}_{RW}^H\mathbf{\Theta}_R\mathbf{g}_{AR}$ can be approximated as a circularly symmetric complex Gaussian RV with mean 0 and variance K, i.e.,

$$\xi_{AW} = \mathbf{g}_{RW}^H\mathbf{\Theta}_R\mathbf{g}_{AR} \sim \mathcal{CN}(0, K), \tag{19}$$

Proof: Under the optimal reflection coefficients matrix $\mathbf{\Theta}_R^*$ of STAR-RIS, ξ_W can be rewritten as

$$\begin{aligned}\xi_{AW} &= \mathbf{g}_{RW}^H \mathbf{\Theta}_R \mathbf{g}_{AR} \\ &= \sum_{k=1}^{K} \mid g_{RW,k} \mid\mid g_{AR,k} \mid e^{j\left(\theta_{RW,k}+\theta_{AR,k}+\left(\theta_k^R\right)^*\right)} \\ &= \sum_{k=1}^{K} \mid g_{RW,k} \mid\mid g_{AR,k} \mid e^{j(\theta_{RW,k}+\theta_{AB}-\theta_{RB,k})}, \end{aligned} \quad (20)$$

which is the sum of K out-of-phase complex-valued coefficients. It is noting that $\theta_{RW,k}$, θ_{AB} and $\theta_{RB,k}$ are i.i.d. RVs circularly uniformly distributed on $[0, 2\pi)$, so their weighted combination follows the same uniform distribution $U[0, 2\pi)$. In the light of the central limit theorem (CLT), ξ_W can be approximated as a 0-mean complex Gaussian RV. By means of [Lemma 4, [15]] and Appendix C in [16], the probability distribution of ξ_W can be acquired when K is sufficiently large. The approximation is verified to be tight even with relatively small K in [16]. ∎

Lemma 2: When K is sufficiently large, $\xi_L = \mathbf{g}_{RL}^H \mathbf{\Theta}_T \mathbf{g}_{AR}$ can be approximated as a circularly-symmetric complex Gaussian RV with mean 0 and variance K, i.e.,

$$\xi_{AL} = \mathbf{g}_{RL}^H \mathbf{\Theta}_T \mathbf{g}_{AR} \sim \mathcal{CN}(0, K). \quad (21)$$

Proof: Similar to the proof of *Lemma* 1. ∎

Based on *Lemma* 1, $\sigma_{\nu_1}^2$ can be reconstructed as

$$\begin{aligned}\sigma_{\nu_1}^2 &= P_A \mid \sqrt{L_{AW}} g_{AW} + \sqrt{L_{AR} L_{RW}} \mathbf{g}_{RW}^H \mathbf{\Theta}_R \mathbf{g}_{AR} \mid^2 \\ &= P_A (L_{AW} + K L_{AR} L_{RW}) \mid \xi_0 \mid^2, \end{aligned} \quad (22)$$

where $\xi_0 \sim \mathcal{CN}(0, 1)$. As such, $\sigma_{\nu_1}^2$ can be regarded as an exponential RV with expectation $\lambda_{W1} = P_A(L_{AW} + KL_{AR}L_{RW})$, i.e.,

$$\sigma_{\nu_1}^2 \sim \exp\left(\frac{1}{\lambda_{W1}}\right) = \exp\left(\frac{1}{P_A(L_{AW} + KL_{AR}L_{RW})}\right). \quad (23)$$

Similarly, based on *Lemma* 2, $\sigma_{\nu_2}^2$ can be also regarded as an exponential RV and its probability distribution is given by

$$\sigma_{\nu_2}^2 \sim \exp\left(\frac{1}{\lambda_{W2}}\right) = \exp\left(\frac{1}{P_A K L_{AR} L_{RL}}\right). \quad (24)$$

Based on the above analysis, we can derive the expected values of $\mathcal{D}\left(\mathbb{P}_0^{W1/W2} \parallel \mathbb{P}_1^{W1/W2}\right)$ over all channel realizations shown in the following theorems.

Theorem 1: The expected value of $\mathcal{D}\left(\mathbb{P}_0^{W1} \parallel \mathbb{P}_1^{W1}\right)$ over all realization of $\sigma_{\nu_1}^2$ can be calculated as

$$\mathcal{E}_{W1} = -\left(1 + \frac{\sigma_W^2}{\lambda_{W1}}\right) \exp\left(\frac{\sigma_W^2}{\lambda_{W1}}\right) \mathrm{Ei}\left(-\frac{\sigma_W^2}{\lambda_{W1}}\right) - 1, \quad (25)$$

where $\mathrm{Ei}(x) = \int_{-\infty}^{x} e^t/t dt$ is the exponential integral function [eq. (8.211), [40]].

Proof: The pdf of $\sigma_{\nu_1}^2$ is expressed as $f_{\sigma_{\nu_1}^2}(x) = \frac{1}{\lambda_{W1}} \exp\left(-\frac{1}{\lambda_{W1}} x\right)$, for $x \geq 0$. Based on this, $\mathcal{E}_{W1}$ can be computed by

$$\begin{aligned}\mathcal{E}_{W1} &= \mathbb{E}\left(\mathcal{D}\left(\mathbb{P}_0^{W1} \parallel \mathbb{P}_1^{W1}\right)\right) \\ &= \underbrace{\int_0^\infty \ln\left(1 + \frac{x}{\sigma_W^2}\right) f_{\sigma_{\nu_1}^2}(x) dx}_{\mathcal{E}_{11}} + \underbrace{\int_0^\infty \frac{\sigma_W^2 f_{\sigma_{\nu_1}^2}(x)}{x + \sigma_W^2} dx}_{\mathcal{E}_{12}} - 1, \end{aligned} \quad (26)$$

where

$$\begin{aligned}\mathcal{E}_{11} &= \int_0^\infty \ln\left(1 + \frac{x}{\sigma_W^2}\right) \frac{1}{\lambda_{W1}} \exp\left(-\frac{1}{\lambda_{W1}} x\right) dx \\ &\overset{(b)}{=} -\exp\left(\frac{\sigma_W^2}{\lambda_{W1}}\right) \mathrm{Ei}\left(-\frac{\sigma_W^2}{\lambda_{W1}}\right) \end{aligned} \quad (27)$$

and

$$\begin{aligned}\mathcal{E}_{12} &= \int_0^\infty \frac{\sigma_W^2}{x + \sigma_W^2} \frac{1}{\lambda_{W1}} \exp\left(-\frac{1}{\lambda_{W1}} x\right) dx \\ &\overset{(c)}{=} -\frac{\sigma_W^2}{\lambda_{W1}} \exp\left(\frac{\sigma_W^2}{\lambda_{W1}}\right) \mathrm{Ei}\left(-\frac{\sigma_W^2}{\lambda_{W1}}\right), \end{aligned} \quad (28)$$

in which [eq. (4.337-2), [40]] and [eq. (3.352-4), [40]] are utilized at (b) and (c), respectively. Substituting (27) and (28) into (26), the closed-form expression of $\mathcal{E}_{W1}$ is derived. The proof is completed. ∎

Theorem 2: The expected value of $\mathcal{D}\left(\mathbb{P}_0^{W2} \parallel \mathbb{P}_1^{W2}\right)$ over all realization of $\sigma_{\nu_2}^2$ can be calculated as

$$\mathcal{E}_{W2} = -\left(1 + \frac{\sigma_W^2}{\lambda_{W2}}\right) \exp\left(\frac{\sigma_W^2}{\lambda_{W2}}\right) \mathrm{Ei}\left(-\frac{\sigma_W^2}{\lambda_{W2}}\right) - 1. \quad (29)$$

Proof: Similar to the proof of *Theorem 1*. ∎

Based on *Theorem 1* and *Theorem 2*, in the following, the covertness of the STAR-RIS assisted downlink NOMA networks can be evaluated by means of the following constraints:

$$\mathcal{E}_{W1} \leq 2\varepsilon^2, \quad \text{and} \quad \mathcal{E}_{W2} \leq 2\varepsilon^2. \quad (30)$$

C. Covert STAR-RIS Downlink NOMA Design

In this subsection, we first analyze the reliability of STAR-RIS assisted downlink NOMA networks. Upon this, an ECR maximization problem is formulated, subject to the covertness and reliability constraints. By solving this, the optimal system parameters can be acquired.

1) Reliability Analysis: According to the coherent phase shift shown in (8) and (9), the cascade channels of Bob and Cindy can be respectively rewritten as

$$\begin{aligned}\xi_B &= \sqrt{L_{AB}} g_{AB} + \sqrt{L_{AR} L_{RB}} \mathbf{g}_{RB}^H \mathbf{\Theta}_R \mathbf{g}_{AR} \\ &= \sqrt{L_{AB}} \mid g_{AB} \mid + \sqrt{L_{AR} L_{RB}} \sum_{k=1}^{K} \mid g_{AR} \mid\mid g_{RB} \mid, \end{aligned} \quad (31)$$

and

$$\begin{aligned}\xi_C &= \sqrt{L_{AR} L_{RC}} \mathbf{g}_{RC}^H \mathbf{\Theta}_T \mathbf{g}_{AR} \\ &= \sqrt{L_{AR} L_{RC}} \sum_{k=1}^{K} \mid g_{AR} \mid\mid g_{RC} \mid. \end{aligned} \quad (32)$$

In the following, we analyze the distributions of the cascade channels.

Lemma 3: When K is sufficiently large, $\mid \xi_B \mid^2$ can be approximated as a Gamma RV with shape k_B and scale θ_B, i.e.,

$$\mid \xi_B \mid^2 \sim \Gamma(k_B, \theta_B), \tag{33}$$

where $k_B = \frac{K\mu_B^2}{4\delta_B^2}$, $\theta_B = 4K\delta_B^2$, $\mu_B = \sqrt{\frac{L_{AB}\pi}{2K^2}} + \sqrt{L_{AR}L_{RB}}\Omega_{m_{AB}}$, $\delta_B^2 = \frac{L_{AB}(4-\pi)}{2K^2} + L_{AR}L_{RB}\left(1-\Omega_{m_{AB}}^2\right)$ and $\Omega_{m_{AB}} = \frac{\Gamma\left(m_{AR}+\frac{1}{2}\right)\Gamma\left(m_{RB}+\frac{1}{2}\right)}{\Gamma(m_{AR})\Gamma(m_{RB})(m_{AR}m_{RB})^{1/2}}$.

Proof: See proof in Appendix A. The approximation is verified to be tight even if $K = 4$ in [22]. ∎

Lemma 4: When K is sufficiently large, $\mid \xi_C \mid^2$ can be approximated as a Gamma RV with shape k_C and scale θ_C, i.e.,

$$\mid \xi_C \mid^2 \sim \Gamma(k_C, \theta_C), \tag{34}$$

where $k_B = \frac{K\mu_C^2}{4\delta_C^2}$, $\theta_C = 4K\delta_C^2$, $\mu_C = \sqrt{L_{AR}L_{RC}}\Omega_{m_{AC}}$, $\delta_C^2 = L_{AR}L_{RC}(1-\Omega_{m_{AC}}^2)$ and $\Omega_{m_{AC}} = \frac{\Gamma\left(m_{AR}+\frac{1}{2}\right)\Gamma\left(m_{RC}+\frac{1}{2}\right)}{\Gamma(m_{AR})\Gamma(m_{RC})(m_{AR}m_{RC})^{1/2}}$.

Proof: See proof in Appendix B. ∎

When decoding SINRs or SNRs at terminals are less than preset values, the information transmissions will be interrupted in the STAR-RIS assisted downlink network. To guarantee the reliability of covert communications, the interruption probability should be controlled within a small range. Assume that the preset target rates of Bob and Cindy are respectively R_B and R_C. Following, we analyze the interruption probabilities of Bob and Cindy in detail.

Theorem 3: The interruption probability decoding x_B at Bob under the imperfect SIC can be given by

$$\begin{aligned}\mathcal{P}_B =& 1 - \left(1 - \frac{1}{\Gamma(k_B)}\gamma\left(k_B, \frac{\sigma_0^2 r_C}{\theta_B(a_2 - a_1 r_C)P_A}\right)\right) \\ &\times \left(1 - \frac{1}{\Gamma(k_B)}\gamma\left(k_B, \frac{\sigma_0^2 r_B}{\theta_B(a_1 - \phi a_2 r_B)P_A}\right)\right),\end{aligned} \tag{35}$$

where $r_B = 2^{R_B} - 1$ and $r_C = 2^{R_C} - 1$. $\Gamma(x) = \int_0^\infty e^{-t}t^{x-1}dt$ and $\gamma(a,x) = \int_0^x e^{-t}t^{a-1}dt$ are the gamma function [eq. (8.310-1), [40]] and the lower incomplete gamma function [eq. (8.350-1), [40]], respectively.

Proof: See proof in Appendix C. ∎

Theorem 4: The interruption probability decoding x_C at Cindy can be given by

$$\mathcal{P}_C = \frac{1}{\Gamma(k_C)}\gamma\left(k_C, \frac{\sigma_0^2 r_C}{\theta_C(a_2 - a_1 r_C)P_A}\right). \tag{36}$$

Proof: See proof in Appendix D. ∎

2) Covert Transmission Principle: In the downlink network, Alice aims to transmit two covert signals to Bob and Cindy under the help of the STAR-RIS without being detected by wardens. The ECR of the downlink network can be defined as $C_{cov}^D = (1-\mathcal{P}_B)R_B + (1-\mathcal{P}_C)R_C$. To improve the covert performance of the STAR-RIS assisted downlink NOMA network, we maximize the ECR of the network by jointly optimizing the transmit power P_A and power allocation coefficient a_1, subject to reliability constraints of Bob and Cindy, covertness constraints of the network and the boundary constraints. As such, the optimization problem can be formulated as

$$\max_{a_1, P_A} \; C_{cov}^D = (1-\mathcal{P}_B)R_B + (1-\mathcal{P}_C)R_C \tag{37a}$$

$$s.t. \; \mathcal{E}_{W1} \le 2\varepsilon^2, \tag{37b}$$

$$\mathcal{E}_{W2} \le 2\varepsilon^2, \tag{37c}$$

$$\mathcal{P}_B \le p_B, \tag{37d}$$

$$\mathcal{P}_C \le p_C, \tag{37e}$$

$$0 < a_1 < 0.5, \text{ and } a1 + a2 = 1 \tag{37f}$$

$$0 < P_A \le p_{max}, \tag{37g}$$

in which (37b) and (37c) are the covertness constraints of the network. (37d) and (37e) are the reliability constraints with p_B and p_C being the tolerable maximum interruption probabilities at Bob and Cindy, respectively. (37f) and (37g) are the boundary constraints of a_1 and P_A, respectively. p_{max} is the maximum transmit power at Alice. Because of $\frac{d\gamma(a,x)}{dx} = x^{a-1}e^{-x} > 0$, it is easy to prove that $\mathcal{P}_B$ and $\mathcal{P}_C$ are two monotonically decreasing functions w.r.t. P_A. The ECR $\mathcal{C}_{cov}^D$ is a monotonically increasing function w.r.t. P_A. As such, the value of P_A should be as large as possible. Note that $\mathcal{E}_{W1}, \mathcal{E}_{W2}$ are only related to P_A but a_1. We analyze the monotonicity of $\mathcal{E}_{W1}, \mathcal{E}_{W2}$ on P_A in the following.

Lemma 5: $\mathcal{E}_{W1}, \mathcal{E}_{W2}$ are two monotonically increasing functions with respect to P_A.

Proof: See proof in Appendix E. ∎

In the light of *Lemma* 5, (37b) and (37c) can be rewritten as $P_A \le P_A^\dagger$ and $P_A \le P_A^\ddagger$ with $P_A^\dagger$ and $P_A^\ddagger$ being the solutions $\mathcal{E}_{W1}(P_A) = 2\varepsilon^2$ and $\mathcal{E}_{W2}(P_A) = 2\varepsilon^2$ respectively. Synthetically, Larger P_A, smaller the interruption probabilities and larger ECR. The optimal value P_A is determined by the covertness constraints and can be given by

$$P_A^* = \min\left(p_{max}, P_A^\dagger, P_A^\ddagger\right). \tag{38}$$

For given optimal P_A, the optimization problem (37) can be reformulated as

$$\begin{aligned}\min_{a_1} \; & C_{cov,1}^D = \mathcal{P}_B R_B + \mathcal{P}_C R_C \\ s.t. \; & \text{(37d), (37e) and (37f).}\end{aligned} \tag{39}$$

Note that $\mathcal{P}_C$ is a monotonically increasing function a_1, so (37e) can be rewritten as $a_1 \le a_1^\dagger$ with $a_1^\dagger$ being the solution $\mathcal{P}_C(a_1) = p_C$. (37e) and (37f) is jointly equivalent to $0 < a_1 \le \min(a_1^\dagger, 0.5)$ and $a_1 + a_2 = 1$. Owing to the complicated expressions of (35) and $C_{cov,1}^D$, it is difficult to derive their derivatives w.r.t. a_1 to perform the Lagrange duality method. (39) can be solved by a 1-D numerical search over the interval $(0, \min(a_1^\dagger, 0.5))$ efficiently. Resultantly, substituting the optimal a_1^* and P_A^* into C_{cov}^D, the maximum ECR of the downlink network can be acquired.

IV. Covert Communications in STAR-RIS Uplink NOMA Networks

In this section, we consider the covert communications in the STAR-RIS assisted uplink NOMA networks. First, we analyze the information transmission of the uplink NOMA networks. Then, we detail the covertness of the networks. Last, the covert transmission scheme is designed.

A. STAR-RIS Assisted Uplink NOMA Transmissions

As shown in Fig. 1(b), in the uplink NOMA network, Bob and Cindy transmit two unit-power covert signals x_B and x_C with the help of a STAR-RIS. The received signals at Alice can be denoted by

$$\begin{aligned} y_A[m] = &\left(\sqrt{L_{AB}}g_{AB} + \sqrt{L_{AR}L_{RB}}\mathbf{g}_{AR}^H\boldsymbol{\Theta}_R'\mathbf{g}_{RB}\right)\times \\ &\sqrt{P_B}x_B[m] + \sqrt{L_{AR}L_{RB}P_C}\mathbf{g}_{AR}^H\boldsymbol{\Theta}_T'\mathbf{g}_{RC}x_C[m] \\ &+ n_A[m], \end{aligned} \tag{40}$$

where P_B and P_C are the transmit powers at Bob and Cindy, respectively. Assume that cascade channel between Bob and Alice is better than that between Cindy and Alice, so the signal of Cindy can be allocated more power, i.e., $P_C > P_B$. $n_A \sim \mathcal{CN}(0, \sigma_0^2)$ is the AWGN at Alice. $\boldsymbol{\Theta}_R' = \text{diag}\left(e^{j\theta_1'^R}, ..., e^{j\theta_k'^R}, ..., e^{j\theta_K'^R}\right) \in \mathbb{C}^{K\times K}$ and $\boldsymbol{\Theta}_T' = \text{diag}\left(e^{j\theta_1'^T}, ..., e^{j\theta_k'^T}, ..., e^{j\theta_K'^T}\right) \in \mathbb{C}^{K\times K}$ denote the reflection and refraction coefficients matrixes of the STAR-RIS in the uplink NOMA networks. Similar to the downlink NOMA networks, in order to maximize the SNRs decoding the covert signals at Alice, a coherent phase shift strategy is performed at the STAR-RIS [22]. Because of the channel reciprocity, the optimal reflection and refraction coefficients matrixes can be given by

$$\boldsymbol{\Theta}_R'^* = \boldsymbol{\Theta}_R^* \text{ and } \boldsymbol{\Theta}_T'^* = \boldsymbol{\Theta}_T^*. \tag{41}$$

As such, the cascade channels between Alice and users in the uplink NOMA networks are the same as those in downlink NOMA network in Sect. III. We denote the cascade channels from Bob to Alice and from Cindy to Alice by $\xi_B = \sqrt{L_{AB}}g_{AB} + \sqrt{L_{AR}L_{RB}}\mathbf{g}_{AR}^H\boldsymbol{\Theta}_R'\mathbf{g}_{RB}$ and $\xi_C = \sqrt{L_{AR}L_{RC}}\mathbf{g}_{AR}^H\boldsymbol{\Theta}_T'\mathbf{g}_{RC}$. Considering imperfect SIC, Alice first decode the signal of Cindy x_C by regarding the signal of Bob x_B as the interference, and then extract the signal of Bob x_B by removing the partial x_C. The SINR decoding x_C and SINR extracting x_B at Alice can be denoted by

$$\gamma_{A,C} = \frac{|\,\xi_C\,|^2\,P_C}{|\,\xi_B\,|^2\,P_B + \sigma_0^2}, \tag{42}$$

and

$$\gamma_{A,B} = \frac{|\,\xi_B\,|^2\,P_B}{\varphi\,|\,\xi_C\,|^2\,P_C + \sigma_0^2}, \tag{43}$$

respectively. $0 \le \varphi < 1$ is the imperfect SIC factor at Alice with $\varphi = 0$ meaning the perfect SIC.

B. Covertness Analysis of STAR-RIS Uplink NOMA

1) Detection at Wardens: In the STAR-RIS assisted uplink NOMA networks, there are Willie 1 and Willie 2 monitoring the transmission behaviours of Bob and Cindy respectively. As long as one of two wardens detects transmission, the communication is exposed. Assume that the transmissions of Bob and Cindy are synchronized through the synchronization frame command interaction. In a given slot, Bob and Cindy send the covert information with a equal prior probability $\rho = 0.5$. Wardens need to judge whether Bob and Cindy transmit the covert signals based on their observations. Let $\mathcal{H}_0'$ and $\mathcal{H}_1'$ respectively represent that Bob and Cindy send the covet messages or not. Under $\mathcal{H}_0'$ and $\mathcal{H}_1'$, the received signals at Willie 1 and Willie 2 can be given as follows:

$$\begin{cases} \mathcal{H}0' : y_{W1}'[m] = n_{W1}'[m], \\ \mathcal{H}0' : y_{W2}'[m] = n_{W2}'[m], \\ \mathcal{H}1' : y_{W1}'[m] = \sqrt{L_{RW}L_{RC}P_C}\mathbf{g}_{RW}^H\boldsymbol{\Theta}_T'\mathbf{g}_{RC}x_C[m] \\ \qquad + \left(\sqrt{L_{BW}}g_{BW} + \sqrt{L_{RW}L_{RB}}\mathbf{g}_{RW}^H\boldsymbol{\Theta}_R'\mathbf{g}_{RB}\right) \\ \qquad \times \sqrt{P_B}x_B[m] + n_{W1}'[m], \\ \mathcal{H}1' : y_{W2}'[m] = \sqrt{L_{RL}L_{RB}P_B}\mathbf{g}_{RL}^H\boldsymbol{\Theta}_T'\mathbf{g}_{RB}x_B[m] \\ \qquad + \left(\sqrt{L_{CL}}g_{CL} + \sqrt{L_{RL}L_{RC}}\mathbf{g}_{RL}^H\boldsymbol{\Theta}_R'\mathbf{g}_{RC}\right) \\ \qquad \times \sqrt{P_C}x_C[m] + n_{W2}'[m]. \end{cases} \tag{44}$$

Wherein, $n_{W1}' \sim \mathcal{CN}(0, \sigma_W^2)$ and $n_{W2}' \sim \mathcal{CN}(0, \sigma_W^2)$ denote the AWGN at Willie 1 and Willie 2, respectively. As analyzed in III-B, the KL divergence is adopted to evaluate the covertness. Under $\mathcal{H}0'$ and $\mathcal{H}1'$, the probability distributions of received signals at Willie 1/Willie 2 can be given as follows: $\mathbb{P}_0'^{W1} \triangleq f(y_{W1}'[m]|\mathcal{H}0) = \mathcal{CN}(0, \sigma_W^2)$, $\mathbb{P}_0'^{W2} \triangleq f(y_{W2}'[m]|\mathcal{H}0) = \mathcal{CN}(0, \sigma_W^2)$, $\mathbb{P}_1'^{W1} \triangleq f(y_{W1}'[m]|\mathcal{H}1) = \mathcal{CN}(0, |\sqrt{L_{RW}L_{RC}}\mathbf{g}_{RW}^H\boldsymbol{\Theta}_T'\mathbf{g}_{RC}|^2P_C + |(\sqrt{L_{BW}}g_{BW} + \sqrt{L_{RW}L_{RB}}\mathbf{g}_{RW}^H\boldsymbol{\Theta}_R'\mathbf{g}_{RB}|^2P_B + \sigma_W^2)$ and $\mathbb{P}_1'^{W2} \triangleq f(y_{W2}'[m]|\mathcal{H}1) = \mathcal{CN}(0, |\sqrt{L_{RL}L_{RB}}\mathbf{g}_{RL}^H\boldsymbol{\Theta}_T'\mathbf{g}_{RB}|^2P_B + |(\sqrt{L_{CL}}g_{CL} + \sqrt{L_{RL}L_{RC}}\mathbf{g}_{RL}^H\boldsymbol{\Theta}_R'\mathbf{g}_{RC}|^2P_C + \sigma_W^2)$. Based on those, the KL divergences for Willie 1 and Willie 2 can be respectively calculated as

$$\mathcal{D}_{W1}' = \ln\left(1 + \frac{\sigma_{\nu_1}'^2}{\sigma_W^2}\right) + \frac{\sigma_W^2}{\sigma_{\nu_1}'^2 + \sigma_W^2} - 1, \tag{45}$$

and

$$\mathcal{D}_{W2}' = \ln\left(1 + \frac{\sigma_{\nu_2}'^2}{\sigma_W^2}\right) + \frac{\sigma_W^2}{\sigma_{\nu_2}'^2 + \sigma_W^2} - 1, \tag{46}$$

where $\sigma_{\nu_1}'^2$ and $\sigma_{\nu_2}'^2$ can be respectively given by

$$\begin{aligned} \sigma_{\nu_1}'^2 = &|\sqrt{L_{BW}}g_{BW} + \sqrt{L_{RW}L_{RB}}\mathbf{g}_{RW}^H\boldsymbol{\Theta}_R'\mathbf{g}_{RB}|^2P_B \\ &+ P_C|\sqrt{L_{RW}L_{RC}}\mathbf{g}_{RW}^H\boldsymbol{\Theta}_T'\mathbf{g}_{RC}|^2, \end{aligned} \tag{47}$$

and

$$\begin{aligned} \sigma_{\nu_2}'^2 = &|\sqrt{L_{CL}}g_{CL} + \sqrt{L_{RL}L_{RC}}\mathbf{g}_{RL}^H\boldsymbol{\Theta}_R'\mathbf{g}_{RC}|^2P_C \\ &+ P_B|\sqrt{L_{RL}L_{RB}}\mathbf{g}_{RL}^H\boldsymbol{\Theta}_T'\mathbf{g}_{RB}|^2. \end{aligned} \tag{48}$$

2) Expected Detection Performance: Having no access to the instantaneous CSI of wardens, the expectation of the KL divergence is analyzed to evaluate the covertness of the networks. Following, we first analyze the probability distribution of $\sigma_{\nu_1}'^2$ and $\sigma_{\nu_1}'^2$.

Lemma 6: When K is sufficiently large, $\xi_{BW} = \mathbf{g}_{RW}^H\boldsymbol{\Theta}_R'\mathbf{g}_{RB}$, $\xi_{BL} = \mathbf{g}_{RL}^H\boldsymbol{\Theta}_T'\mathbf{g}_{RB}$, $\xi_{CL} = \mathbf{g}_{RL}^H\boldsymbol{\Theta}_R'\mathbf{g}_{RC}$ and $\xi_{CW} = \mathbf{g}_{RW}^H\boldsymbol{\Theta}_T'\mathbf{g}_{RC}$ can be approximated as four circularly symmetric complex Gaussian RVs with mean 0 and variance K, i.e.,

$$\xi_{BW}, \xi_{BL}, \xi_{CL}, \xi_{CW} \sim \mathcal{CN}(0, K). \tag{49}$$

Proof: Similar to the proof of *Lemma* 1. ■

Based on Lemma 6, $\sigma_{\nu_1}^{\prime 2}$ can be rewritten as

$$\sigma_{\nu_1}^{\prime 2} = P_B(L_{BW} + KL_{RW}L_{RB})|\delta_0|^2 + P_C KL_{RW}L_{RC}|\delta_1|^2, \tag{50}$$

where $|\delta_0|^2, |\delta_1|^2 \sim \mathcal{CN}(0,1)$. Denoting $\lambda_{BW} = P_B(L_{BW} + KL_{RW}L_{RB})$ and $\lambda_{CW} = P_C KL_{RW}L_{RC}$, the pdf of $\sigma_{\nu_1}^{\prime 2}$ can be calculated as

$$f_{\sigma_{\nu_1}^{\prime 2}}(x) = \frac{1}{\lambda_{CW} - \lambda_{BW}} \left(e^{-\frac{x}{\lambda_{CW}}} - e^{-\frac{x}{\lambda_{BW}}} \right). \tag{51}$$

Similarly, the pdf of $\sigma_{\nu_2}^{\prime 2}$ can be calculated as

$$f_{\sigma_{\nu_2}^{\prime 2}}(x) = \frac{1}{\lambda_{BL} - \lambda_{CL}} \left(e^{-\frac{x}{\lambda_{BL}}} - e^{-\frac{x}{\lambda_{CL}}} \right), \tag{52}$$

where $\lambda_{CL} = P_C(L_{CL} + KL_{RL}L_{RC})$ and $\lambda_{BL} = P_B KL_{RL}L_{RB}$, the pdf of $\sigma_{\nu_1}^{\prime 2}$. In the light of above analysis, the expectations of the KL divergences over all channels realizations can be shown in the following theorem.

Theorem 5: The expected values of $\mathcal{D}\left(\mathbb{P}_0^{\prime W1} \parallel \mathbb{P}_1^{\prime W1}\right)$ over all realization of $\sigma_{\nu_1}^{\prime 2}$ and $\mathcal{D}\left(\mathbb{P}_0^{\prime W2} \parallel \mathbb{P}_1^{\prime W2}\right)$ over all realization of $\sigma_{\nu_2}^{\prime 2}$ can be respectively given by

$$\mathcal{E}_{W1}' = \frac{\lambda_{BW} + \sigma_W^2}{\lambda_{CW} - \lambda_{BW}} \exp\left(\frac{\sigma_W^2}{\lambda_{BW}}\right) \mathrm{Ei}\left(-\frac{\sigma_W^2}{\lambda_{BW}}\right) - \frac{\lambda_{CW} + \sigma_W^2}{\lambda_{CW} - \lambda_{BW}} \exp\left(\frac{\sigma_W^2}{\lambda_{CW}}\right) \mathrm{Ei}\left(-\frac{\sigma_W^2}{\lambda_{CW}}\right) - 1, \tag{53}$$

and

$$\mathcal{E}_{W1}' = \frac{\lambda_{CL} + \sigma_W^2}{\lambda_{BL} - \lambda_{CL}} \exp\left(\frac{\sigma_W^2}{\lambda_{CL}}\right) \mathrm{Ei}\left(-\frac{\sigma_W^2}{\lambda_{CL}}\right) - \frac{\lambda_{BL} + \sigma_W^2}{\lambda_{BL} - \lambda_{CL}} \exp\left(\frac{\sigma_W^2}{\lambda_{BL}}\right) \mathrm{Ei}\left(-\frac{\sigma_W^2}{\lambda_{BL}}\right) - 1. \tag{54}$$

.

Proof: Similar to the proof of *Theorem* 1. ∎

In line with *Theorem* 5, in the following, the covertness of the STAR-RIS assisted uplink NOMA networks can be evaluated by means of the following constraints:

$$\mathcal{E}_{W1}' \le 2\varepsilon^2, \quad \text{and} \quad \mathcal{E}_{W2}' \le 2\varepsilon^2. \tag{55}$$

C. Covert STAR-RIS Uplink NOMA Design

In this subsection, we first characterize the interruption performance of STAR-RIS assisted uplink NOMA networks. On this basis, an optimization problem to maximize the ECR of the uplink networks is formulated, under the constraints of covertness and reliability. Solving this, the optimal transmit powers at terminals can be gotten.

1) Reliability Analysis: Because of the channel reciprocity, cascade channels between Alice and Bob/Cindy in the uplink NOMA networks are the same as those in the downlink NOMA networks. The probability distributions of cascade channels can refer to *Lemma* 3 and *Lemma* 4. The cascade channel from Bob to Alice is better than that from Cindy to Alice, so Alice first decodes the signal of Cindy and then extract the signal of Bob by employing imperfect SIC. When the SINR decoding x_C or the SNR extracting x_B is below the preset value, the networks will be interrupted. The interruption probabilities at Alice can be derived in the following theorem.

Theorem 6: The interruption probabilities decoding x_C and x_B at Alice can be given by

$$\mathcal{P}_{A,C} = 1 - \frac{1}{\Gamma(k_B)} \exp\left(-\frac{r_C\sigma_0^2}{\theta_C P_C}\right) \left\{ \sum_{m_1=0}^{k_C-1} \sum_{n_1=1}^{N_a} \frac{\omega_{n_1}}{m_1!} x_{n_1}^{k_B-1} \times \left(\frac{r_C P_B \theta_B x_{n_1} + r_C\sigma_0^2}{\theta_C P_C} \right)^{m_1} \exp\left(-\frac{r_C P_B \theta_B x_{n_1}}{\theta_C P_C}\right) \right\}, \tag{56}$$

and

$$\mathcal{P}_{A,B} = 1 - \left\{ \frac{1}{\Gamma(k_B)} \exp\left(-\frac{r_C\sigma_0^2}{\theta_C P_C}\right) \sum_{m_1=0}^{k_C-1} \sum_{n_1=1}^{N_a} \frac{\omega_{n_1}}{m_1!} x_{n_1}^{k_B-1} \left(\frac{r_C P_B \theta_B x_{n_1} + r_C\sigma_0^2}{\theta_C P_C} \right)^{m_1} \exp\left(-\frac{r_C P_B \theta_B x_{n_1}}{\theta_C P_C}\right) \right\} \times \left\{ \frac{1}{\Gamma(k_C)} \exp\left(-\frac{\varphi r_B\sigma_0^2}{\theta_B P_B}\right) \sum_{m_2=0}^{k_B-1} \sum_{n_2=1}^{N_a} \frac{\omega_{n_2}}{m_2!} x_{n_2}^{k_C-1} \left(\frac{\varphi r_B P_C \theta_C x_{n_2} + r_B\sigma_0^2}{\theta_B P_B} \right)^{m_2} \exp\left(-\frac{\varphi r_B P_C \theta_C x_{n_2}}{\theta_B P_B}\right) \right\}, \tag{57}$$

respectively. Wherein, $\omega_i = \frac{x_i}{(n+1)^2 (L_{n+1}(x_i))^2}$ and $L_n(x) = \frac{1}{n!}(\frac{d}{dx} - 1)^n x^n$ being the Laguerre polynomials [41]. x_i is i-th root of $L_n(x)$.

Proof: See proof in Appendix F. ∎

2) Covert Transmission Principle: In the uplink NOMA network, Bob and Cindy attempt to covertly transmit the information to Alice aided by a STAR-RIS. The ECR for the uplink networks can be defined as $C_{cov}^U = (1-\mathcal{P}_{A,B})R_B + (1-\mathcal{P}_{A,C})R_C$. In order to improve the network performance, an ECR maximization problem is formulated by jointly optimizing the transmit power of the users, subject to the covertness demands of the network, the reliability constraints of the users and maximum power constraint. The optimization problem can be described as

$$\max_{P_B, P_C} \; C_{cov}^U = (1 - \mathcal{P}_{A,B})R_B + (1 - \mathcal{P}_{A,C})R_C \tag{58a}$$

$$s.t. \; \mathcal{E}_{W1}' \le 2\varepsilon^2, \tag{58b}$$

$$\mathcal{E}_{W2}' \le 2\varepsilon^2, \tag{58c}$$

$$\mathcal{P}_{A,B} \le p_B, \tag{58d}$$

$$\mathcal{P}_{A,C} \le p_C, \tag{58e}$$

$$0 < P_B + P_C \le p_{max} \text{ and } P_B < P_C, \tag{58f}$$

where p_{max} is the maximum scheduling power of uplink networks. The descriptions of other parameters are the same as those in Sect. IV-B. (58b) and (58c) are the covertness demands of the uplink network. (58d) and (58e) are the reliability constraints of uplink users. (58f) is the total power constraint of the network. Because of the complicated expressions of (53), (54), (56) and (57) and the coupled variables, it is difficult to acquire the closed-form solutions of the non-convex problem. To tackle with it, we transform (56) into a two-dimensional problem with specific bounds. Letting $P_B = \beta P_U$ and $P_C = (1-\beta)P_U$, (58f) can be equivalently converted to

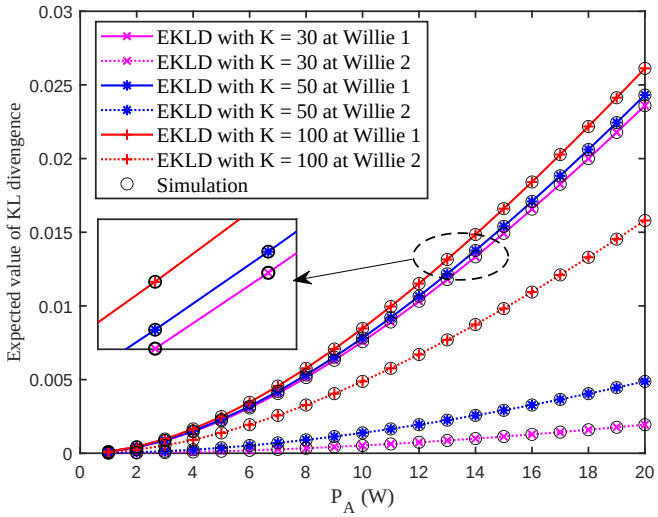

Fig. 3. $\mathcal{E}_{W1}$ and $\mathcal{E}_{W2}$ v.s. P_A for the different K in the STAR-RIS downlink NOMA networks.

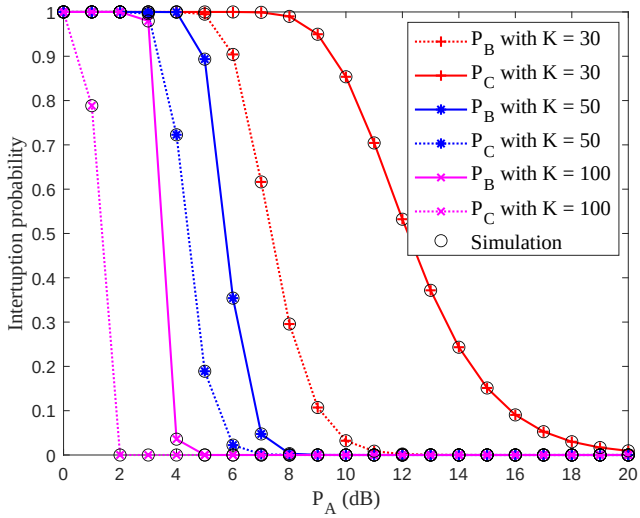

Fig. 4. $\mathcal{P}_B$ and $\mathcal{P}_C$ v.s. P_A for the different K in the STAR-RIS downlink NOMA network.

$0 < P_U \leq p_{max}$ and $0 < \beta < 0.5$. As such, (58) can be reformulated as

$$\max_{P_U,\beta} \; C_{cov}^{U} = (1-\mathcal{P}_{A,B})R_B + (1-\mathcal{P}_{A,C})R_C \tag{59a}$$

$$s.t. \;\; 0 < P_U \leq p_{max} \text{ and } 0 < \beta < 0.5, \tag{59b}$$

(58b), (58c), (58d) and (58e).

which can be solved by a 2-D numerical search over the intervals $(0, 0.5)$ and $(0, p_{max}]$. It is noted that the 2-D numerical search is efficient since the lower and upper bounds β and P_U are explicitly given. Substituting the optimal β^* and P_U^* into $P_B = \beta P_U$ and $P_C = (1-\beta)P_U$, the optimal P_B^* and P_C^* are gotten. Resultantly, the maximum ECR of the uplink network can be acquired.

V. Numerical Results and Discussions

In this section, numerical results are provided to validated the proposed scheme for the downlink and uplink NOMA networks. For evaluating the superiority of the proposed scheme in terms of the effective covert rate, this paper considers three benchmarks: STAR-RIS assisted OMA scheme, the relay assisted NOMA scheme and the relay assisted OMA scheme.

A. STAR-RIS Downlink NOMA Networks

Unless otherwise specified, the system parameters for the downlink networks will be set as follows: $m_\Delta = 2$, $\beta = 3$, $\phi = 0.1$, $\sigma_w^2 = \sigma_0^2 = 0.1$ W, $r_c = 0.4$ bps/Hz, $r_b = 0.6$ bps/Hz, $p_B = p_C = 0.1$, $d_{ab} = d_{rc} = 5$ and $d_{ar} = d_{aw} = d_{rw} = d_{rb} = d_{rl} = 10$.

Fig. 3 shows the relationships between $\mathcal{E}_{W1}$ and $\mathcal{E}_{W2}$ and P_A for different K in the downlink NOMA networks, in which EKLD means the expected values of KL divergence for the downlink networks: $\mathcal{E}_{W1}$ or $\mathcal{E}_{W2}$. It can be found from Fig. 3 that both $\mathcal{E}_{W1}$ and $\mathcal{E}_{W2}$ are proportional to P_A. When the transmit power increases, Willie 1 and Willie 2 are more likely to detect the information transmissions. This results in reduced detection error probabilities at Willie 1 and Willie 2 and thus increased $\mathcal{E}_{W1}$ and $\mathcal{E}_{W2}$, which means the transmit power should be controlled according the covertness demand. Also, it is observed from Fig. 3 that both $\mathcal{E}_{W1}$ and $\mathcal{E}_{W2}$ are proportional to K. This is because the bigger K, the better the channels quality of Willie 1 and Willie 2 and the smaller the detection error probabilities. Additionally, simulation results verify the accuracy of the theoretical results.

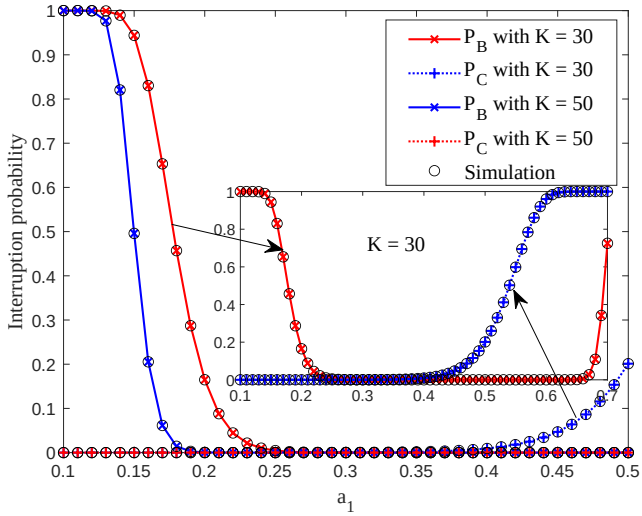

Fig. 5. $\mathcal{P}_B$ and $\mathcal{P}_C$ v.s. a_1 for the different K in the STAR-RIS downlink NOMA network.

Figs. 4 and 5 demonstrate the relationships between the interruption probabilities and P_A with a_1, respectively. It is observed that both $\mathcal{P}_B$ and $\mathcal{P}_C$ are inversely proportional to P_A. As P_A increases, the power of signals received at Bob and Cindy increases. As such, the users can more easily decode the signals, which makes $\mathcal{P}_B$ and $\mathcal{P}_C$ smaller. For Bob and

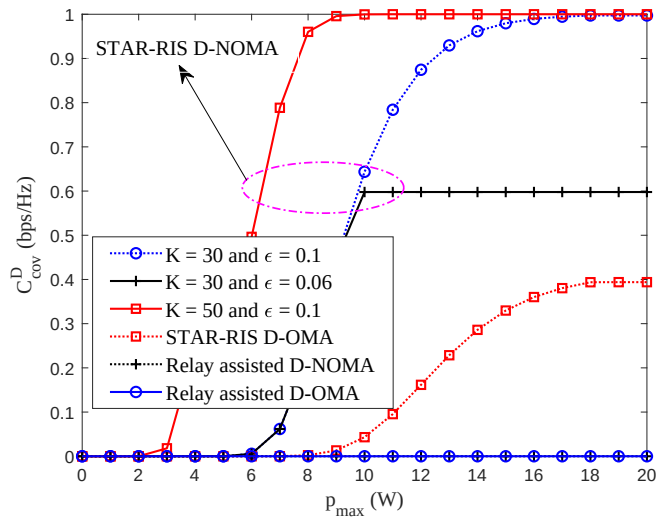

Fig. 6. C_{cov}^{D} for the different schemes in the downlink networks.

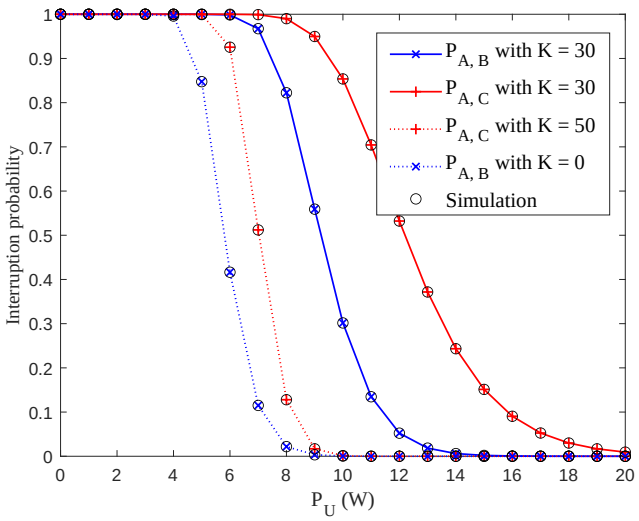

Fig. 8. $\mathcal{P}_{A,B}$ and $\mathcal{P}_{A,C}$ v.s. P_U for the different K in the STAR-RIS uplink NOMA network.

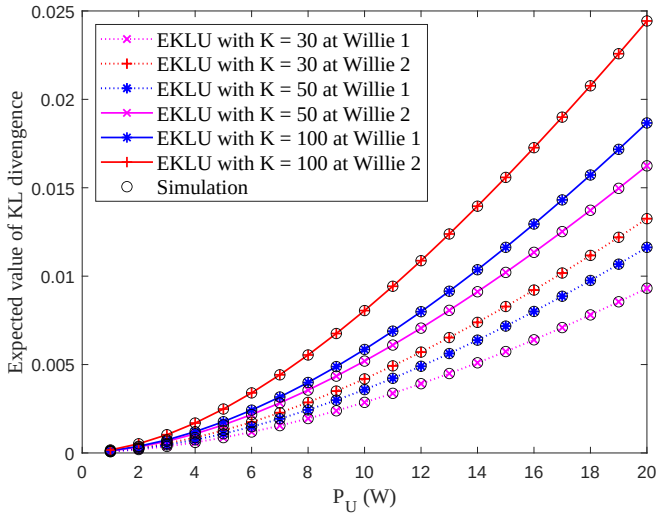

Fig. 7. $\mathcal{E}'_{W1}$ and $\mathcal{E}'_{W2}$ v.s. P_U for the different K in the STAR-RIS uplink NOMA networks.

Cindy, P_A should be set as large as possible. Fig. 5 shows that $\mathcal{P}_B$ first decreases and then increases and $\mathcal{P}_C$ increases with an increase of a_1. As a_1 increases, more power is allocated to x_B and less power is allocated to x_C. As a result, it gets harder for Cindy to decode x_C and thus $\mathcal{P}_C$ gets bigger. For Bob, he needs to first decoded x_C and then x_B. With the increasing a_1, decoding x_C gets more easily. When a_1 increases to a specific value, e.g. $a_1 = 0.66$ shown in the Fig. 5, Bob decodes x_C with a decoding error, causing $\mathcal{P}_B$ to increase first and then decrease. In a real system, a_1 should be set within $(0, 0.5)$ for user fairness and the reliability demands. From the Figs. 4 and 5, it is also found that $\mathcal{P}_B$ and $\mathcal{P}_C$ are inversely proportional to K, which demonstrates that RIS can enhance the reliability of the networks. Also, analysis results are verified by simulations.

Fig. 6 compares the effective covert rate of the proposed scheme and three benchmarks. In the figure, D-OMA and D-NOMA respectively means the downlink OMA and NOMA. We can find that the proposed STAR-RIS assisted D-NOMA scheme outperforms three benchmarks in terms of the effective covert rate C_{cov}^{D}. This is because, for the STAR-RIS assisted D-OMA scheme, its covertness is the same as the proposed scheme, but its interruption performance is weaker than the proposed scheme without the NOMA. For the relay assisted D-NOMA and D-OMA scheme, the power of multiple observations at wardens is the same without the phase or power uncertainty. Once Alice sends the signals, wardens can detect the existence of the communications, so the effective covert rates are equal to 0. Fig. 6 also shows the trend of C_{cov}^{D} with respect to the maximum transmit power p_{max} for the different covertness demands ε. It is observed that C_{cov}^{D} will reach its maximum value and level off when p_{max} grows to a certain value for the different ε. In addition, when ε is smaller, C_{cov}^{D} cannot reach its maximum. This is because when the covertness demand is higher, Alice cannot send signals with too much power, otherwise the transmissions will be detected by wardens.

B. STAR-RIS Uplink NOMA Networks

Fig. 7 depicts the relationships between $\mathcal{E}'_{W1}$ and $\mathcal{E}'_{W2}$ and the total power P_U of the uplink networks. We can find that both $\mathcal{E}'_{W1}$ and $\mathcal{E}'_{W2}$ increase with P_U. The reason is that the more power in the network, the more power received by wardens, and the more likely wardens can successfully detect the communications. To ensure the covertness of the transmissions, P_U should be reasonably selected. Fig. 7 also depicts the effect of K on $\mathcal{E}'_{W1}$ and $\mathcal{E}'_{W2}$ for the uplink networks. The trend and reasons are the same as those in Fig. 5 for the downlink networks. Also, simulation results are provided to verify the analytical results.

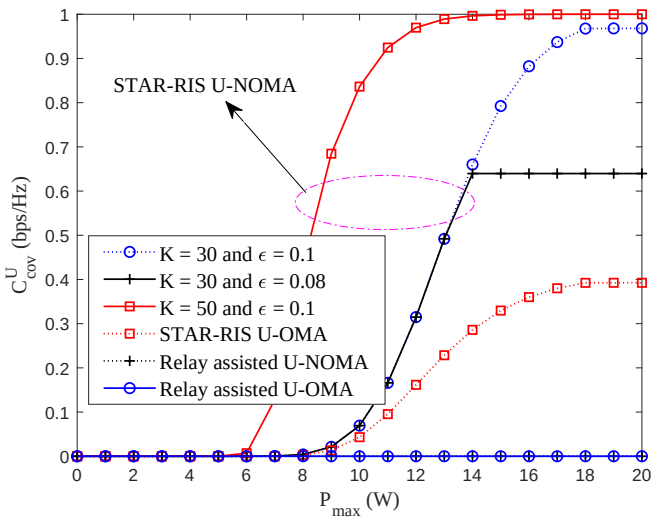

Fig. 9. C_{cov}^{U} for the different schemes in the uplink networks.

Fig. 8 reveals the relationships between the interruption probabilities, $\mathcal{P}_{A,B}$ and $\mathcal{P}_{A,C}$, and the total power P_U for the STAR-RIS assisted uplink NOMA networks. It can be observed from Fig. 8 that both $\mathcal{P}_{A,B}$ and $\mathcal{P}_{A,C}$ reduces with the increase of P_U. The reason is that the bigger P_U, the bigger power allocated to Bob and Cindy, and the easier it is for Alice to decode x_B and x_C. In (58), a balance between the reliability and the covertness is made by adjusting P_U for the uplink networks. It is also observed that K can improve the interruption performance of the uplink networks. At last, analytical results are verified by simulations.

Fig. 9 compares the effective covert rate C_{cov}^{U} of the proposed scheme and three benchmarks. In the figure, U-OMA and U-NOMA respectively denotes the uplink OMA and NOMA. It is observed from Fig. 9 that the effective covert rate of the proposed scheme is greater than those of three benchmarks. For the STAR-RIS assisted U-OMA scheme, the decoding SINR of Alice is below that using the NOMA protocol. For relay assisted U-OMA and U-NOMA schemes, multiple observations are the same without phase or power uncertainty. Once transmitted, wardens can detect the communication successfully. Fig. 9 also indicates that C_{cov}^{U} first increases to its maximum and then tends to be stable with the increase of the maximum scheduling power p_{max} of uplink networks. In addition, we can find that C_{cov}^{U} cannot reach its maximum when the covertness demand is higher.

VI. Conclusion

This paper considered the covert communication in STAR-RIS assisted NOMA networks over Nakagami-m fading channels for downlink and uplink IoT scenarios. Under the NOMA protocol with the imperfect SIC, an IoT access point attempted to achieve information interaction with two IoT users aided by a STAR-RIS. The two IoT users were located at both sides of STAR-RIS, where Bob was the near user and Cindy was the far user. Bob and Cindy were monitored by Willie 1 and Willie 2, respectively. The phase shifting of STAR-RIS provided users a shelter for covert transmissions. In this paper, KL divergence was used to evaluate the detection performance of wardens. The cascade channels gains of users and wardens were respectively approximated as Gamma and complex Gaussian RV. Without the instantaneous CSI of wardens, the expectations of KL divergence were characterized. In order to measure the reliability, the interruption probabilities of the networks were derived. For the downlink scenario, by jointly optimizing the transmit power and power allocation coefficient of the IoT access point, the ECR of the downlink networks was maximized. For the uplink scenario, by jointly the transmit power of users, the ECR of the uplink networks was maximized. The two maximization problems were respectively solved analytically, subject to the covertness demands, reliability constraints and power boundary constraints. Finally, simulation results showed that applying STAR-RIS into NOMA IoT networks could bring more covertness gain as compared with benchmarks.

Appendix A
Proof of Lemma 3

According to (31), ξ_B can be restructured as

$$\xi_B = \sqrt{L_{AB}} \mid g_{AB} \mid + \sqrt{L_{AR}L_{RB}} \sum_{k=1}^{K} \mid g_{AR} \mid\mid g_{RB} \mid$$
$$= \sum_{k=1}^{K} \left(\sqrt{\frac{L_{AB}}{K^2}} |g_{AB}| + \sqrt{L_{AR}L_{RB}} |g_{AR}||g_{RB}| \right). \quad (60)$$

Denote $h_{AB} = \sqrt{\frac{L_{AB}}{K^2}} |g_{AB}| + \sqrt{L_{AR}L_{RB}} |g_{AR}||g_{RB}|$. We can calculate the expectation and variance of h_{AB} respectively as

$$\mathbb{E}(h_{AB}) = \sqrt{\frac{L_{AB}\pi}{2K^2}} + \sqrt{L_{AR}L_{RB}}\Omega_{m_{AB}}, \quad (61)$$

and

$$\mathbb{V}(h_{AB}) = \frac{L_{AB}(4-\pi)}{2K^2} + L_{AR}L_{RB}\left(1 - \Omega_{m_{AB}}^2\right), \quad (62)$$

In line with the CLT, ξ_B can be approximated as a Gaussian RV distributed on $\mathcal{N}(K\mathbb{E}(h_{AB}), K\mathbb{V}(h_{AB}))$. By means of [*Corollary 1*, [22]], *Lemma 3* can be proved.

Appendix B
Proof of Lemma 4

Denote $h_{AC} = \sqrt{L_{AR}L_{RC}} \mid g_{AR} \mid\mid g_{RC} \mid$. The expectation and variance of h_{AC} can be respectively calculated as

$$\mathbb{E}(h_{AC}) = \sqrt{L_{AR}L_{RC}}\Omega_{m_{AC}}, \quad (63)$$

and

$$\mathbb{V}(h_{AC}) = L_{AR}L_{RC}(1 - \Omega_{m_{AC}}^2), \quad (64)$$

In line with the CLT, ξ_C can be approximated as a Gaussian RV distributed on $\mathcal{N}(K\mathbb{E}(h_{AC}), K\mathbb{V}(h_{AC}))$. By means of [*Corollary 1*, [22]], *Lemma 4* can be proved.

Appendix C
Proof of Theorem 3

It is assumed that Bob has better channel condition, so Bob first decodes x_C and then extract x_B by removing x_C.

Considering the imperfect SIC, the interruption probability at Bob can be calculated by

$$\mathcal{P}_B = 1 - \mathbb{P}(\gamma_{B,C} > r_C)\mathbb{P}(\gamma_B > r_B), \tag{65}$$

where

$$\begin{aligned}\mathbb{P}(\gamma_{B,C} > r_C) &= \mathbb{P}\left(\frac{|\xi_B|^2 a_2 P_A}{|\xi_B|^2 a_1 P_A + \sigma_0^2} > r_C\right) \\ &= \mathbb{P}\left(|\xi_B|^2 > \frac{\sigma_0^2 r_C}{(a_2 - a_1 r_C)P_A}\right) \\ &\overset{(d)}{=} 1 - \frac{1}{\Gamma(k_B)}\gamma\left(k_B, \frac{\sigma_0^2 r_C}{\theta_B(a_2 - a_1 r_C)P_A}\right),\end{aligned} \tag{66}$$

and

$$\begin{aligned}\mathbb{P}(\gamma_B > r_B) &= \mathbb{P}\left(\frac{|\xi_B|^2 a_1 P_A}{\phi|\xi_B|^2 a_2 P_A + \sigma_0^2} > r_B\right) \\ &= \mathbb{P}\left(|\xi_B|^2 > \frac{\sigma_0^2 r_B}{(a_1 - \phi a_2 r_B)P_A}\right) \\ &\overset{(d)}{=} 1 - \frac{1}{\Gamma(k_B)}\gamma\left(k_B, \frac{\sigma_0^2 r_B}{\theta_B(a_1 - \phi a_2 r_B)P_A}\right),\end{aligned} \tag{67}$$

where (d) means utilizing the distribution probability of $|\xi_B|^2$ in the integral. Substituting (66) and (67) into (65), the close-form expression of $\mathcal{P}_B$ is gotten and *Theorem* 3 is proved.

Appendix D
Proof of Theorem 4

As far user, regarding x_B as the interference, Cindy directly decodes x_C. Based on *Lemma 4*, the interruption probability at Cindy can be calculated by

$$\begin{aligned}\mathcal{P}_C = \mathbb{P}(\gamma_C < r_C) &= \mathbb{P}\left(\frac{|\xi_C|^2 a_2 P_A}{|\xi_C|^2 a_1 P_A + \sigma_0^2} < r_C\right) \\ &= \mathbb{P}\left(|\xi_C|^2 < \frac{\sigma_0^2 r_C}{(a_2 - a_1 r_C)P_A}\right) \\ &= \frac{1}{\Gamma(k_C)}\gamma\left(k_C, \frac{\sigma_0^2 r_C}{\theta_C(a_2 - a_1 r_C)P_A}\right).\end{aligned} \tag{68}$$

As such, we complete the proof.

Appendix E
Proof of Lemma 5

Denote $b(x) = -(1+x)\exp(x)\mathrm{Ei}(-x)$, for $x > 0$. The first derivative of $b(x)$ w.r.t. x can be calculated by

$$\begin{aligned}\frac{db(x)}{dx} &= -\left((x+2)\exp(x)\mathrm{Ei}(-x) + \frac{x+1}{x}\right) \\ &= (x+2)e^x\left(\int_x^\infty \frac{\exp(-t)}{t}dt - \frac{x+1}{x(x+2)\exp(x)}\right).\end{aligned} \tag{69}$$

Denote $c(x) = (x+1)/(x(x+2)\exp(x))$, its first derivative w.r.t. x can be calculated as

$$\frac{dc(x)}{dx} = \frac{\exp(-x)(-2 - x(x+2)^2)}{x^2(x+2)^2} \tag{70}$$

It is noting that $\frac{dc(x)}{dx}$ is continuous for $x > 0$, so we have

$$\int_x^\infty \frac{e^{-t}(-2 - t(t+2)^2)}{t^2(t+2)^2}dt = c(\infty) - c(x) = -c(x). \tag{71}$$

Substituting (71) into (69), $\frac{db(x)}{dx}$ can be rewritten as

$$\frac{db(x)}{dx} = (x+2)e^x\int_x^\infty \frac{-2\exp(-t)}{t^2(t+2)^2}dt, \tag{72}$$

which is always less than or equal to 0 for $x > 0$, so $b(x)$ is a monotonically decreasing function w.r.t. x. $\mathcal{E}_{W1} = b\left(\frac{\sigma_W^2}{\lambda_{W1}}\right) = b\left(\frac{\sigma_W^2}{P_A(L_{AW} + KL_{AR}L_{RW})}\right)$ is a monotonically increasing function w.r.t. P_A. Similarly, $\mathcal{E}_{W2}$ is also a monotonically increasing function w.r.t. P_A. The proof is completed.

Appendix F
Proof of Theorem 6

At Alice, x_C is first decoded. Based on (42), the interruption probability decoding x_C at Alice can be calculated by

$$\begin{aligned}\mathcal{P}_{A,C} &= \mathbb{P}(\gamma_{A,C} < r_C) = \mathbb{P}\left(\frac{|\,\xi_C\,|^2\,P_C}{|\,\xi_B\,|^2\,P_B + \sigma_0^2} < r_C\right) \\ &= \int_0^\infty \int_0^{\frac{r_C P_B}{P_C}y + \frac{r_C\sigma_0^2}{P_C}} f_{|\xi_C|^2}(x) f_{|\xi_B|^2}(y)dxdy \\ &= \int_0^\infty \frac{1}{\Gamma(k_C)}\gamma\left(k_C, \frac{r_C P_B x + r_C\sigma_0^2}{P_C}\right)\frac{x^{k_B-1}e^{-\frac{x}{\theta_B}}}{\Gamma(k_B)\theta_B^{k_B}}dx \\ &= 1 - \int_0^\infty e^{-\frac{r_C P_B x + r_C\sigma_0^2}{\theta_C P_C}}\sum_{m_1=0}^{k_C-1}\frac{1}{m_1!}\left(\frac{r_C P_B x + r_C\sigma_0^2}{\theta_C P_C}\right)^{m_1} \\ &\qquad \times \frac{x^{k_B-1}e^{-\frac{x}{\theta_B}}}{\Gamma(k_B)\theta_B^{k_B}}dx \\ &\overset{(e)}{=} 1 - \frac{1}{\Gamma(k_B)}\exp\left(-\frac{r_C\sigma_0^2}{\theta_C P_C}\right)\left\{\sum_{m_1=0}^{k_C-1}\sum_{n_1=1}^{N_a}\frac{\omega_{n_1}}{m_1!}x_{n_1}^{k_B-1}\right. \\ &\qquad \left.\times\left(\frac{r_C P_B\theta_B x_{n_1} + r_C\sigma_0^2}{\theta_C P_C}\right)^{m_1}\exp\left(-\frac{r_C P_B\theta_B x_{n_1}}{\theta_C P_C}\right)\right\},\end{aligned} \tag{73}$$

where the Gauss-Laguerre quadrature [eq. (25.4.45), [41]] is used in (e). Under the imperfect SIC, the interruption probability decoding x_B at Alice can be calculated by

$$\begin{aligned}\mathcal{P}_{A,B} &= 1 - \mathbb{P}(\gamma_{A,C} > r_C)\mathbb{P}(\gamma_{A,B} > r_B) \\ &= 1 - (1 - \mathbb{P}(\gamma_{A,C} < r_C))(1 - \mathbb{P}(\gamma_{A,B} < r_B)),\end{aligned} \tag{74}$$

where $\mathbb{P}(\gamma_{A,B} < r_B)$ can be calculated similar to (73). With some straightforward algebraic manipulations, *Theorem* 6 can be proved.

References

[1] D. Zhou et al., "Aerospace Integrated Networks Innovation for Empowering 6G: A Survey and Future Challenges," *IEEE Commun. Surv. Tutor.*, early access, Feb. 2023.

[2] D. C. Nguyen, M. Ding ang P. N. Pathirana et al., "6G Internet of Things: A Comprehensive Survey," *IEEE Internet Things J.*, vol. 9, no. 1, pp. 359-383, 1 Jan.1, 2022.

[3] F. Guo et al., "Enabling Massive IoT Toward 6G: A Comprehensive Survey," *IEEE Internet Things J.*, vol. 8, no. 15, pp. 11891-11915, 1 Aug. 2021.

[4] N. -N. Dao et al., "Survey on Aerial Radio Access Networks: Toward a Comprehensive 6G Access Infrastructure," *IEEE Commun. Surv. Tutor.*, vol. 23, no. 2, pp. 1193-1225, Feb, 2021.

[5] Z. Ding et al., "A State-of-the-Art Survey on Reconfigurable Intelligent Surface-Assisted Non-Orthogonal Multiple Access Networks," *Proc. IEEE*, vol. 110, no. 9, pp. 1358-1379, Sep. 2022

[6] O. Maraqa et al., "A Survey of Rate-Optimal Power Domain NOMA With Enabling Technologies of Future Wireless Networks," *IEEE Commun. Surv. Tutor.*, vol. 22, no. 4, pp. 2192-2235, Aug. 2020.

[7] Y. Bai et al., "Prior Information Aided Deep Learning Method for Grant-Free NOMA in mMTC," *IEEE J. Sel. Areas Commun.*, vol. 40, no. 1, pp. 112-126, Jan. 2022.

[8] X. Mu et al., "Intelligent Reflecting Surface Enhanced Multi-UAV NOMA Networks," *IEEE J. Sel. Areas Commun.*, vol. 39, no. 10, pp. 3051-3066, Oct. 2021.

[9] Y. Liu et al., "ptimization of Grant-Free NOMA With Multiple Configured-Grants for mURLLC," *IEEE J. Sel. Areas Commun.*, vol. 40, no. 4, pp. 1222-1236, Apr. 2022.

[10] Y. Liu et al., "Reconfigurable Intelligent Surfaces: Principles and Opportunities," *IEEE Commun. Surv. Tutor.*, vol. 23, no. 3, pp. 1546-1577, May 2021.

[11] C. Huang et al., "Reconfigurable Intelligent Surfaces for Energy Efficiency in Wireless Communication," *IEEE Trans. Wireless Commun.*, vol. 18, no. 8, pp. 4157-4170, Aug. 2019.

[12] G. Chen et al., "Active IRS Aided Multiple Access for Energy-Constrained IoT Systems," *IEEE Trans. Wireless Commun.*, vol. 22, no. 3, pp. 1677-1694, Mar. 2023.

[13] Z. Chu, P. Xiao, D. Mi, W. Hao, Q. Chen and Y. Xiao, "IRS-Assisted Wireless Powered IoT Network With Multiple Resource Blocks," *IEEE Trans. Commun.*, vol. 71, no. 4, pp. 2335-2350, Apr. 2023.

[14] S. Li et al., "IRS-Assisted Full Duplex Systems Over Rician and Nakagami Fading Channels," *IEEE Open J. Veh. Technol.*, vol. 4, pp. 217-229, Jau. 2023.

[15] B. Tahir et al., "Analysis of Uplink IRS-Assisted NOMA Under Nakagami-m Fading via Moments Matching," *IEEE Wireless Commun. Lett.*, vol. 10, no. 3, pp. 624-628, Mar. 2021.

[16] Z. Ding, R. Schober and H. V. Poor, "On the Impact of Phase Shifting Designs on IRS-NOMA," *IEEE Wireless Commun. Lett.*, vol. 9, no. 10, pp. 1596-1600, Oct. 2020.

[17] T. Wang, F. Fang and Z. Ding, "An SCA and Relaxation Based Energy Efficiency Optimization for Multi-User RIS-Assisted NOMA Networks," *IEEE Trans. Veh. Technol.*, vol. 71, no. 6, pp. 6843-6847, Jun. 2022.

[18] Y. Zou et al., "Machine Learning in RIS-assisted NOMA IoT Networks," *IEEE Internet Things J.*, early access, 2023.

[19] H. Zhang and B. Di, "Intelligent Omni-Surfaces: Simultaneous Refraction and Reflection for Full-Dimensional Wireless Communications," *IEEE Commun. Surv. Tutor.*, vol. 24, no. 4, pp. 1997-2028, Aug. 2022.

[20] C. Wu et al., "Coverage Characterization of STAR-RIS Networks: NOMA and OMA," *IEEE Commun. Lett.*, vol. 25, no. 9, pp. 3036-3040, Sep. 2021.

[21] W. Du et al., "STAR-RIS Assisted Wireless Powered IoT Networks," *IEEE Trans. Veh. Technol.*, early access, 2023.

[22] Z. Xie et al., "STAR-RIS Aided NOMA in Multicell Networks: A General Analytical Framework With Gamma Distributed Channel Modeling," *IEEE Trans. Commun.*, vol. 70, no. 8, pp. 5629-5644, Aug. 2022.

[23] T. Wang et al., "Outage Probability Analysis of STAR-RIS Assisted NOMA Network With Correlated Channels," *IEEE Commun. Lett.*, vol. 26, no. 8, Aug. 2022.

[24] J. Zuo et al., "Joint Design for Simultaneously Transmitting and Reflecting (STAR) RIS Assisted NOMA Systems," *IEEE Trans. Wireless Commun.*, vol. 22, no. 1, pp. 611-626, Jan. 2023.

[25] F. Fang et al., "Energy-Efficient Design of STAR-RIS Aided MIMO-NOMA Networks," *IEEE Trans. Commun.*, vol. 71, no. 1, pp. 498-511, Jan. 2023.

[26] Q. Gao et al., "Joint Location and Beamforming Design for STAR-RIS Assisted NOMA Systems," *IEEE Trans. Commun.*, vol. 71, no. 4, pp. 2532-2546, Apr. 2023.

[27] Y. Su et al., "Joint Location and Beamforming Optimization for STAR-RIS Aided NOMA-UAV Networks," *IEEE Trans. Veh. Technol.*, early access, 2023.

[28] C. Gao et al., "Covert Communication in Relay-Assisted IoT Systems," *IEEE Internet Things J.*, vol. 8, no. 8, pp. 6313-6323, 15 Apr. 2021.

[29] M. Wang et al., "Channel Inversion Power Control Aided Covert Communications in Uplink NOMA Systems," *IEEE Wireless Commun. Lett.*, vol. 11, no. 4, pp. 871-875, Apr. 2022.

[30] L. Tao et al., "Covert Communication in Downlink NOMA Systems With Random Transmit Power," *IEEE Wireless Commun. Lett.*, vol. 9, no. 11, pp. 2000-2004, Nov. 2020.

[31] Z. Duan et al., "Covert Communication in Uplink NOMA Systems under Channel Distribution Information Uncertainty," *IEEE Commun. Lett.*, early access, 2023.

[32] L. Tao et al., "Achieving Covert Communication in Uplink NOMA Systems via Energy Harvesting Jammer," *IEEE Commun. Lett.*, vol. 25, no. 12, pp. 3785-3789, Dec. 2021.

[33] P. Liu et al.,"Joint Information-Theoretic Secrecy and Covertness for UAV-assisted Wireless Transmission With Finite Blocklength," *IEEE Trans. Veh. Technol.*, early access, 2023.

[34] S. Ma et al., "Covert Beamforming Design for Intelligent-Reflecting-Surface-Assisted IoT Networks," *IEEE Internet Things J.*, vol. 9, no. 7, pp. 5489-5501, Apr. 2022.

[35] M. T. Mamaghani and Y. Hong, "Aerial Intelligent Reflecting Surface-Enabled Terahertz Covert Communications in Beyond-5G Internet of Things," *IEEE Internet Things J.*, vol. 9, no. 19, pp. 19012-19033, 1 Oct. 2022.

[36] C. Wang et al., "Intelligent Reflecting Surface-Aided Full-Duplex Covert Communications: Information Freshness Optimization," *IEEE Trans. Wireless Commun.*, early access, 2022.

[37] C. Chen et al., "Performance Analysis and Optimization of IRS-Aided Covert Communication With Hardware Impairments," *IEEE Trans. Veh. Technol.*, vol. 72, no. 4, pp. 5463-5467, Apr. 2023.

[38] L. Lv et al., "Covert Communication in Intelligent Reflecting Surface-Assisted NOMA Systems: Design, Analysis, and Optimization," *IEEE Trans. Wireless Commun.*, vol. 21, no. 3, pp. 1735-1750, Mar. 2022.

[39] L. Yang et al., "Covert Transmission and Secrecy Analysis of RS-RIS-NOMA-Aided 6 G Wireless Communication Systems," *IEEE Trans. Veh. Technol.*, early access, 2023.

[40] A. Jeffrey and D. Zwillinger, *Table of Integrals, Series, and Products*, 7th Edition. Oxford, UK: Academic Press, Elsevier Inc., 2007.

[41] M. Abramowitz and I. A. Stegun, *Handbook of Mathematical Functions with Formulas, Graphs and Mathematical Tables.* NY, USA: Dover, 1972.